Title

Selective targeting of IL2Rβγ combined with radiotherapy triggers CD8- and NK-mediated immunity, abrogating metastasis in HNSCC.

Journal

Cell Reports Medicine, 4(8)

Authors

Gadwa, Jacob

Amann, Maria

Bickett, Thomas

et al.

Publication Date

2023-08-15

DOI

10.1016/j.xcrm.2023.101150

Peer reviewed

Cell Reports
Medicine

Article

Selective targeting of IL2Rβγ combined with radiotherapy triggers CD8- and NK-mediated immunity, abrogating metastasis in HNSCC

Graphical abstract

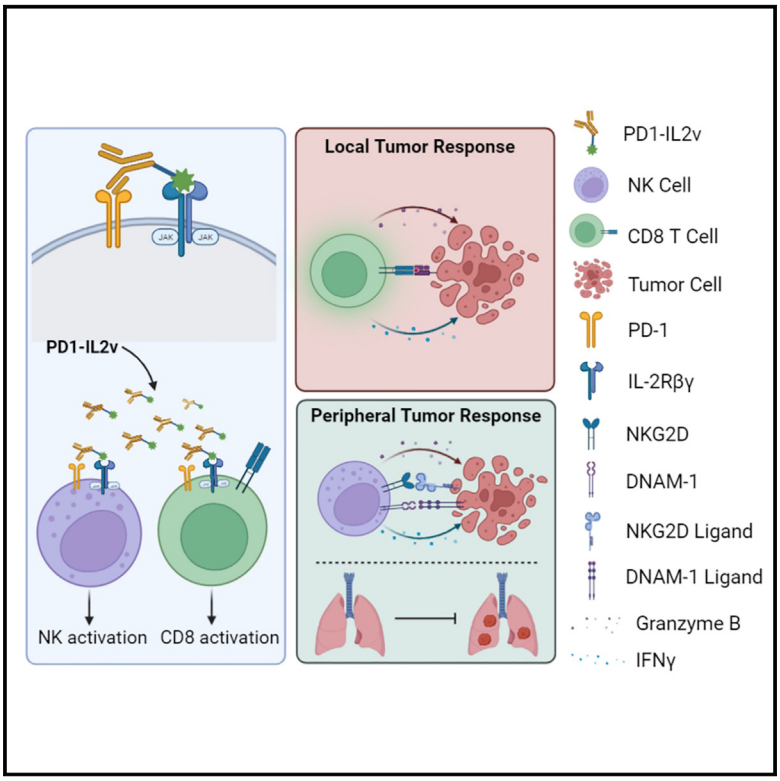

Highlights

- Combined RT and PD1-IL2v drives tumor regression and increases survival
- RT + PD1-IL2v initiates tumor-reactive T cell responses while limiting Treg suppression
- RT + PD1-IL2v enhances NK cell activating receptor expression and cytotoxicity
- Improved NK immunosurveillance controls metastatic spread to lungs

Authors

Jacob Gadwa, Maria Amann, Thomas E. Bickett, ..., Christian Klein, Angelo D'Alessandro, Sana D. Karam

Correspondence

sana.karam@cuanschutz.edu

In brief

In aggressive models of head and neck cancer, Gadwa et al. demonstrate that radiation therapy combined with the immunocytokine PD1-IL2v elicits a robust anti-tumor immune response by invigorating T cell and natural killer cell activation and expansion across multiple immunological compartments, resulting in superior primary and distant tumor control.

Gadwa et al., 2023, Cell Reports Medicine *4*, 101150
August 15, 2023
https://doi.org/10.1016/j.xcrm.2023.101150

CellPress

Cell Reports Medicine

CellPress
OPEN ACCESS

Article

Selective targeting of IL2Rβγ combined with radiotherapy triggers CD8- and NK-mediated immunity, abrogating metastasis in HNSCC

Jacob Gadwa,[1,2] Maria Amann,[3] Thomas E. Bickett,[1] Michael W. Knitz,[1] Laurel B. Darragh,[1,2] Miles Piper,[1] Benjamin Van Court,[1] Sanjana Bukkapatnam,[1] Tiffany T. Pham,[1] Xiao-Jing Wang,[4] Anthony J. Saviola,[5] Laura Codarri Deak,[3] Pablo Umaña,[3] Christian Klein,[3] Angelo D'Alessandro,[5] and Sana D. Karam[1,2,6,*]

[1]Department of Radiation Oncology, University of Colorado, Anschutz Medical Campus, Aurora, CO 80045, USA
[2]Department of Immunology & Microbiology, University of Colorado, Anschutz Medical Campus, Aurora, CO 80045, USA
[3]Roche Innovation Center Zurich, Roche Pharmaceutical Research and Early Development (pRED), 8952 Schlieren, Switzerland
[4]Department of Pathology, University of Colorado, Anschutz Medical Campus, Aurora, CO 80045, USA
[5]Department of Biochemistry and Molecular Genetics, University of Colorado, Anschutz Medical Campus, Aurora, CO 80045, USA
[6]Lead contact
*Correspondence: sana.karam@cuanschutz.edu
https://doi.org/10.1016/j.xcrm.2023.101150

SUMMARY

The implementation of cancer immunotherapies has seen limited clinical success in head and neck squamous cell carcinoma (HNSCC). Interleukin-2 (IL-2), which modulates the survival and functionality of lymphocytes, is an attractive target for new immunotherapies but one that is limited by presence of regulatory T cells (Tregs) expressing the high-affinity IL-2Rα. The bispecific immunocytokine PD1-IL2v preferentially delivers IL-2 signaling through IL-2Rβγ on PD-1-expressing cells. Selectively targeting the intermediate-affinity IL-2Rβγ can be leveraged to induce anti-tumor immune responses in effector T cells and natural killer (NK) cells while limiting the negative regulation of IL-2Rα activation on Tregs. Using radiation therapy (RT) in combination with PD1-IL2v improves local tumor control and survival, and controls metastatic spread in orthotopic HNSCC tumor models. PD1-IL2v drives systemic activation and expansion of circulating and tumor-infiltrating cytotoxic T cells and NK cells while limiting Treg-mediated immunosuppression. These data show that PD1-L2v induces durable systemic tumor control in HNSCC.

INTRODUCTION

The advent of cancer immunotherapy has revolutionized the way oncologists manage and treat cancer, increasing response rates and the overall survival of patients. However, the success of immunotherapies, most notably immune checkpoint inhibitors, is not all-encompassing, with varying levels of efficacy between cancer types or even among patients with the same malignancy.[1] Head and neck squamous cell carcinomas (HNSCCs) are among the most prevalent malignancies worldwide[2] and can be characterized by their immunologically cold tumors and high resistance to therapy, ultimately resulting in poor treatment outcomes.[3] Radiation therapy (RT) is used as standard of care in many cases and, in addition to direct tumor cell kill, helps sensitize the tumor microenvironment (TME) to immunotherapy.[4] Despite these efforts, the development of acquired resistance to combination radioimmunotherapy invariably occurs, with full understanding of the underlying mechanisms yet to be determined.

The immune system plays a fundamental role in disease progression and treatment response in HNSCC.[4,5] Although RT induces an influx of pro-inflammatory immune cells into the TME,[4] this effect is transient, ultimately being dampened by the influx of immunosuppressive regulatory T cells (Tregs).[4,6] Tregs have been identified as key regulators of resistance to radioimmunotherapy[7–9] and, among other mechanisms, can indirectly suppress effector immune function through the sequestration of interleukin-2 (IL-2). Ablation of Tregs using αCD25 can result not only in the activation of CD4 and CD8 T cells but also natural killer (NK) cells, a process that is mediated by IL-2 signaling through IL-2Rβγ.[10,11] NK cells, a class of innate lymphoid cells, play a prominent role in tumor surveillance and direct cytotoxic cell kill both locally and on the periphery.[12,13] Furthermore, NK cells are reliant upon IL-2 signaling for modulating much of their homeostatic and cytotoxic potential,[14,15] making them an enticing target for IL-2-directed immunotherapy.

Immune exhaustion is another confounding factor of acquired resistance.[16] High intratumoral surface expression of programmed cell death protein 1 (PD-1) on lymphocytes coupled with the upregulation of programmed cell death ligand 1 (PD-L1) on tumor cells and suppressive immune cells ensures that tumor-infiltrating lymphocytes are incapable of achieving a sustained anti-tumor response.[4,6,17] While PD-1 blockade has been shown to restore PD-1$^+$ T effector functionality, it also possesses the dichotomous effect of amplifying Treg-mediated

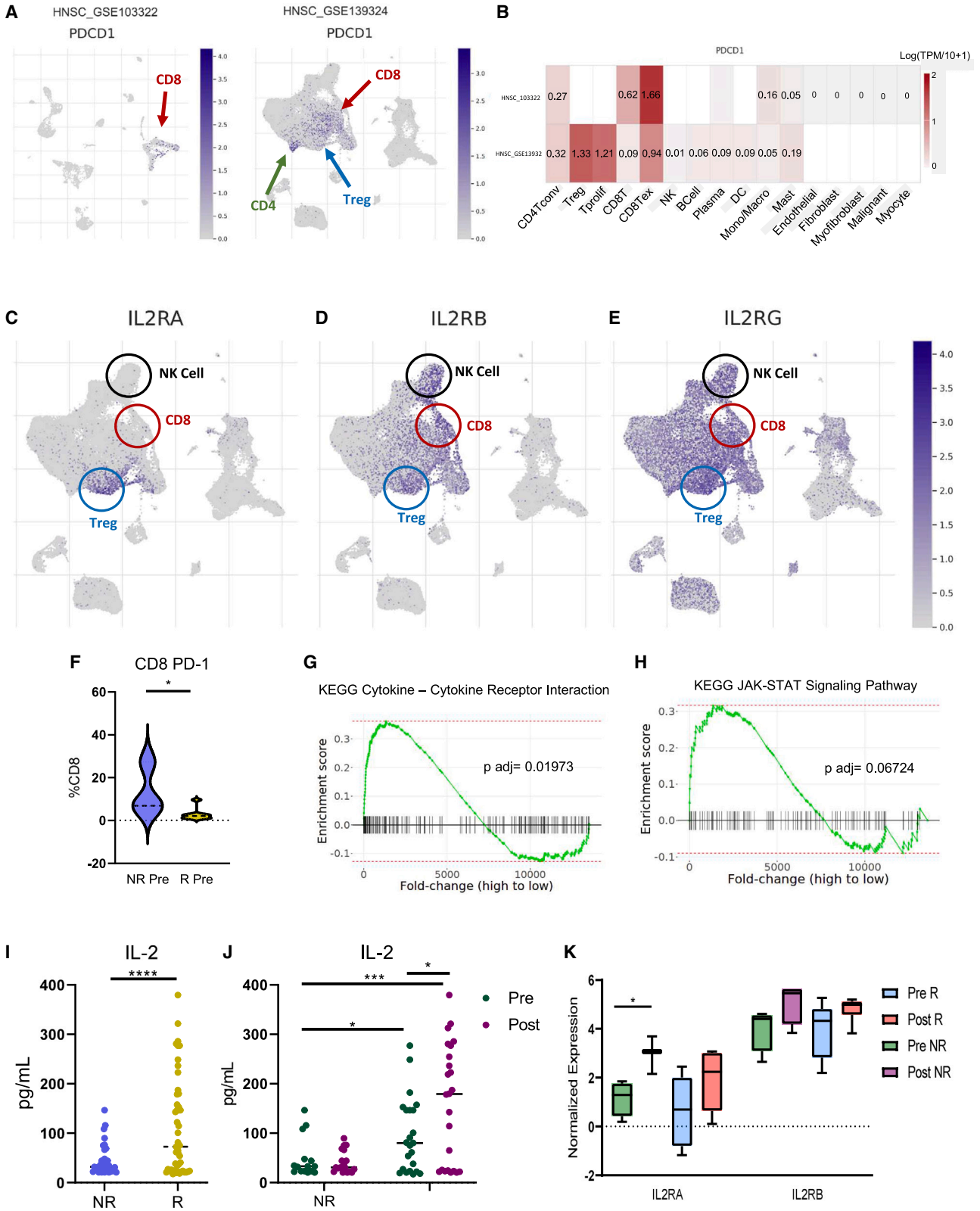

(legend on next page)

immunosuppression among PD-1$^+$ Tregs.[18,19] Therefore, the reactivation of PD-1$^+$ effector T cells with αPD-1 therapy may only be achievable through the subsequent depletion of Tregs.

Here, we investigate the use of PD1-IL2v, a bispecific immunocytokine that activates immune cells via IL-2Rβγ signaling on PD-1-expressing cells,[20] concurrently with a non-IL-2 blocking αCD25 antibody and RT. This, we reasoned, would allow effector T cells to retain functionality without the competitive presence of Tregs, which sequester IL-2 as a means of immunosuppression and can be activated by blockade of PD-1.[18,21] The absence of active Tregs and the increased availability of IL-2 may also serve to activate NK cells via IL-2Rβγ.[10] As NK cells function as critical mediators for immunosurveillance of circulating cancer cells,[22–24] this combination, we hypothesized, could also reduce the formation of distant metastases, a notion of which would hold tremendous therapeutic and translational relevance.

RESULTS

The clinical expression of PD-1 and IL-2 receptors in head and neck cancer

The expression of surface markers on immune cell types helps dictate the subsequent response to immunotherapy.[16] Clinically, the variable expression patterns of immune markers have been well described, with classical exhaustion markers such as PD-1 and CTLA-4 often exhibiting higher prevalence in non-responsive patients.[16] Therapies that can overcome exhaustion and reprogram the TME from an exhausted immunocompromised state to one that is immunocompetent is the next step in developing more efficacious treatments. Examination of PD-1 expression using single-cell RNA sequencing databases of human HNSCC[25,26] (Figures S1A and S1B) reveals PD-1 to be highly clustered on effector CD4 and CD8 T cells, both of which are known to be necessary for effective tumor clearance.[5] At the same time, PD-1 is highly expressed on Tregs (Figures 1A and 1B).

IL-2 receptor signaling is an essential mediator of T cell and NK cell activity and consists of IL-2Rα (CD25), IL-2Rβ (CD122), and IL-2Rγ (CD132), forming a heterotrimeric receptor.[14,27] While IL-2 preferentially signals through the high-affinity IL-2 receptor containing IL-2Rα, signaling through the intermediate-affinity receptor IL-2Rβγ functions heavily in IL-2-mediated activation of effector T cell and NK cell populations.[15] Introduction of an αCD25 antibody has been shown to increase T cell and NK activity, resulting from the depletion of Tregs, which can suppress NK function directly or indirectly through the sequestration of IL-2.[12,13,21,28,29] Examining the IL-2 receptor subunit distribution across immune cell types shows that expression of IL-2Rα is clustered predominantly on Tregs (Figure 1C). IL-2Rβ, however, is more widely distributed among lymphocyte populations, being heavily expressed on CD8 and NK cells (Figure 1D). Meanwhile, IL-2Rγ, which is the common subunit for several type 1 cytokine receptors,[30] is expressed across most cell types (Figure 1E). When assessing the expression among clinical responders and non-responders in a recently completed phase I/Ib clinical trial using neoadjuvant stereotactic body RT (SBRT) with durvalumab,[31] we found that patients exhibited higher frequency of PD-1 expression in post-treatment tumor samples than at the baseline, pre-treatment samples (Figure S1C), with the magnitude of increase being 3-fold higher in non-responders than responders (Figure S1D). Evaluating the PD-1 expression on CD8 T cells revealed significantly higher expression on non-responders at baseline (Figure 1F).

Pathway analysis of RNA sequencing revealed a significant increase in the Kyoto Encyclopedia of Genes and Genomes (KEGG) cytokine-cytokine receptor interaction pathway at baseline in responsive patients (Figure 1G), and a corresponding increase in the KEGG JAK/STAT signaling pathway (Figure 1H), a downstream component of IL-2 receptor signaling.[14] As increased IL-2 signaling in patients could account for superior response to therapy via enhanced effector T cell function, and for the observed increase in JAK/STAT pathway activity, we examined the levels of soluble IL-2 in plasma from patients and observed significantly increased IL-2 availability in responders versus non-responders, both overall and when comparing pre- and post-treatment levels (Figures 1I and 1J). Analyzing expression of IL-2Rα and IL-2Rβ also revealed higher expression of IL-2Rα in non-responders (Figure 1K). Additionally, superior T cell activation was observed in responders, signified by higher levels of zeta chain of T cell receptor associated protein kinase (ZAP70) (Figure S1E). These data collectively suggest that dual targeting of PD-1 and IL-2Rβγ could promote the expansion and survival of effector cells within the TME, helping to overcome acquired resistance and providing therapeutic advantage.

Treatment with PD1-IL2v results in tumor growth delay in HNSCC tumors

To test the hypothesis that targeting both PD-1 and IL-2 signaling concurrently would increase treatment efficacy, we

Figure 1. Clinical expression of PD-1 and IL-2 receptors on lymphocytes in head and neck cancer

(A and B) Cell mapping of HNSCC datasets from TISCH single-cell RNA sequencing database.

(C) Single-cell RNA sequencing of TISCH HNSCC datasets showing PD-1 expression being localized primarily on T cells.

(D) Heatmap showing differential expression of PD-1 across immune cell types gathered from TISCH single-cell RNA sequencing databases.

(E) Single-cell RNA sequencing of IL2 receptor subunit expression on immune cells. Expression is localized to: IL2RA (Treg), IL2RB (CD8, NK cell), and IL2RG (all immune cells).

(F) Expression of PD-1 by CD8 T cells of non-responders (NR) and responders (R) pre-treatment.

(G and H) Enrichment curves for KEGG (G) CYTOKINE_CYTOKINE_RECEPTOR_INTERACTION and (H) KEGG JAK_STAT_SIGNALING_PATHWAY from RNA sequencing data in responder vs. non-responder tumors treated with neoadjuvant SBRT and durvalumab. RNA sequencing on tumors was performed on tumors taken at baseline, pre-treatment time point.

(I and J) Soluble IL-2 expression in pg/mL (I) from human plasma in responders and non-responders and (J) between pre- and post-neoadjuvant and surgery in responders and non-responders.

(K) Normalized RNA sequencing expression of IL2RA and IL2RB in responders and non-responders. Human samples were obtained from 21 patients pre- and post-treatment. Data are presented as mean ± SEM. *$p < 0.05$, **$p < 0.005$, ***$p < 0.0005$, ****$p < 0.0001$.

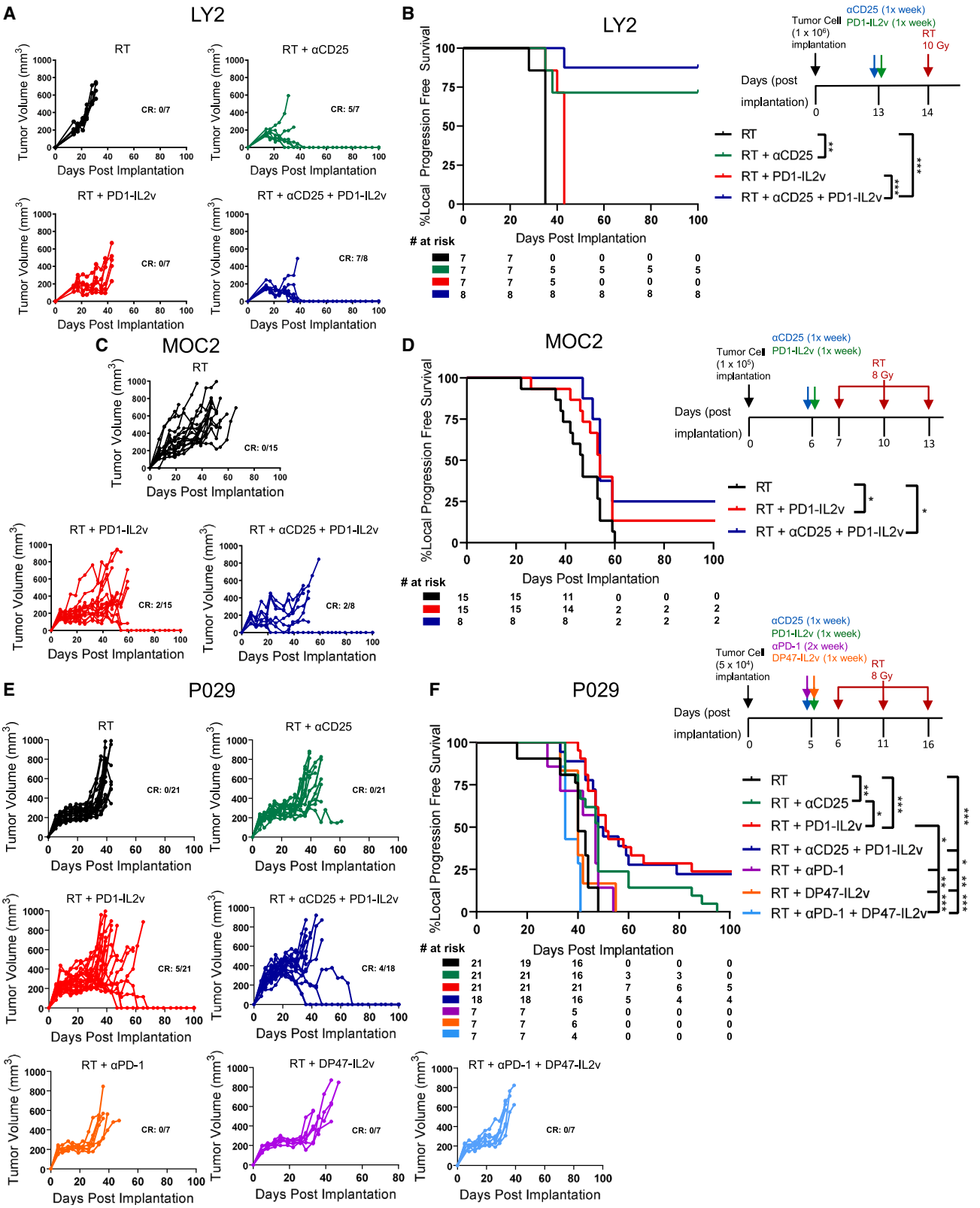

(legend on next page)

utilized the immunocytokine PD1-IL2v, which blocks PD-1 while simultaneously binding IL-2Rβγ on the same cell. The mutated IL2v binding domain is unique in that it is specific to IL-2Rβγ, allowing it to bypass IL-2Rα-mediated Treg activation.[32–34] However, Tregs can also express IL-2Rβγ, and past work has demonstrated that depletion of Tregs helps to overcome radioresistance and improve treatment response. Considering this, we used an αCD25 antibody,[35] optimized to interact with activating Fc receptors to facilitate enhanced depletion of intratumoral Tregs. This approach, we hypothesized, would allow for greater depletion of tumor-infiltrating Tregs while selectively expanding and activating CD25-deficient cells, namely CD8 T cells and NKs.[35]

Consistent with our previous work, the combination of RT and αCD25 eradicated LY2 tumors in approximately 70% of mice. While PD1-IL2v with RT did indeed delay tumor growth, this ultimately did not translate to a significant effect on tumor eradication unless αCD25 is added (Figures 2A, 2B, and S1F). The MOC2 model, on the other hand, was afforded limited, although transient, benefit from αCD25 immunotherapy.[10,36] Given that this tumor model has been historically shown to be dependent on adaptive immunity, particularly CD8 T cells,[7–9] we sought to investigate the impact of PD1-IL2v on tumor growth and survival in MOC2 tumors. We observed significant reduction in tumor growth with the addition of PD1-IL2v to RT, with the addition of αCD25 failing to improve survival (Figures 2C, 2D, and S1G). Confirming these data, we further tested these treatments in the metastatic P029 tumor model. The combination of RT with PD1-IL2v exhibited tumor growth delay (Figures 2E, 2F, and S1H), and survival analysis demonstrated that PD1-IL2v combined with RT provided significant benefit over RT alone or RT + αCD25. Again, the addition of αCD25 to RT + PD1-IL2v did not harbor any additional therapeutic benefit, demonstrating that while tempting, stacking immunotherapies may not necessarily improve overall treatment efficacy. Dissecting the individual components of PD1-IL2v using an αPD-1 antibody and DP47-IL2v (a non-targeted version of the IL2v moiety) revealed that either therapy on its own or in combination failed to elicit any therapeutic benefit (Figures 2E, 2F, and S1H).

Radiation therapy enhances the therapeutic benefit of PD1-IL2v

To isolate the contribution of RT to therapeutic efficacy of PD1-IL2v, we examined the effect of each of the therapeutic arms without RT in LY2, MOC2, and P029 tumors (Figures S1I and S1L). PD1-IL2v without RT did result in tumor growth delay in LY2 and MOC2 models, although the effect lacks durability and the tumors eventually regrow (Figures S1I and S1J). On the other hand, P029 tumors are unresponsive to any form of immunotherapy in the absence of RT (Figures S1K and S1L). Based on these data, we show that RT is required to unlock the full therapeutic benefit of PD1-IL2v in our tumor models.

PD1-IL2v remodels the immune TME and promotes the expansion of effector lymphocytes

Based on the findings that treatment with RT and PD1-IL2v delays growth, with low levels of eradication, we sought to understand the mechanism by which our combination therapy influences the immunological makeup of the TME. We observed significant alterations in three distinct effector populations within the TME of MOC2 tumors when administering PD1-IL2v with RT (Figures 3A–3F). First, we observed an increase in CD4 T cell infiltration into the tumor (Figure 3A), in addition to significant increases in IL-2, interferon-γ (IFNγ), and CD44 (Figure 3B). We also observed an increase in LFA-1 among tumor-infiltrating CD4s, which in addition to its role in T cell trafficking helps tune CD4 responses and polarization toward T helper 1 phenotypes (Figure S2B).[37] CD3ζ is a cytoplasmic signaling component of the T cell receptor (TCR) complex that becomes phosphorylated upon TCR engagement.[38] Levels of phosphorylated CD3ζ significantly increased as a consequence of treatment with PD1-IL2v (Figure 3C). Concordant with the improved effector function, we also observed increased production of IFNγ by Tregs, suggestive of Treg dysfunction (Figure S2C).[39,40] Next, we saw similar influx and activation of CD8 T cells, with increases in granzyme B, IFNγ, and CD44 (Figures 3D and 3E). Lastly, NK cells, previously described as playing an important role in mediating the response to HNSCC,[10] showed significant upregulation of the activating receptors DNAM-1 and NKG2D, along with IFNγ and granzyme B (Figure 3F).

To establish that the effects of PD1-IL2v were not model specific, we further assessed the immunomodulatory effects of PD1-IL2v in the metastatic P029 model. These results paralleled what we observed in MOC2 tumors (Figures S2D–S2F). Notably, elevated expression of CD44 and granzyme B indicates that effector cells in the TME of P029 tumors are more activated and cytotoxic after treatment with PD1-IL2v (Figures 3G and 3H). To reinforce the importance of CD8 T cells in mounting an

Figure 2. Treatment with αCD25 and PD1-IL2v results in tumor growth delay in HNSCC tumor models

(A) Tumor growth curves for mice implanted with LY2 tumors.

(B) Kaplan-Meier survival curve of mice implanted with LY2 tumors and experimental timeline. LY2 tumors were established and treated with either αCD25, PD1-IL2v, αCD25 and PD1-IL2v, or no treatment beginning 1 day prior to RT. RT was delivered as a single dose of 10 Gy. Antibodies were administered weekly via intraperitoneal (i.p.) injection for the duration of the study.

(C) Tumor growth curves for mice implanted with MOC2 tumors.

(D) Kaplan-Meier survival curve of mice implanted with MOC2 tumors and experimental timeline. MOC2 tumors were established and treated with either αCD25, PD1-IL2v, αCD25 and PD1-IL2v, or no treatment beginning 1 day prior to RT. RT was delivered in three fractions of 8 Gy, with 3–4 days between fractions. Antibodies were administered weekly via i.p. injection for the duration of the study.

(E) Tumor growth curves for mice implanted with P029 tumors.

(F) Kaplan-Meier survival curve of mice implanted with P029 tumors and experimental timeline. P029 tumors were established and treated with either αCD25, PD1-IL2v, αCD25 and PD1-IL2v, αPD-1, PD47-IL2v, or αPD-1 and DP47-IL2v, or no treatment beginning 1 day prior to RT. RT was delivered in three fractions of 8 Gy, with 5 days between fractions. Antibodies were administered weekly via i.p. injection for the duration of the study.

n = 7–21 mice per group and represented by multiple pooled experiments. Data are presented as mean ± SEM. *$p < 0.05$, **$p < 0.005$, ***$p < 0.0005$, ****$p < 0.0001$.

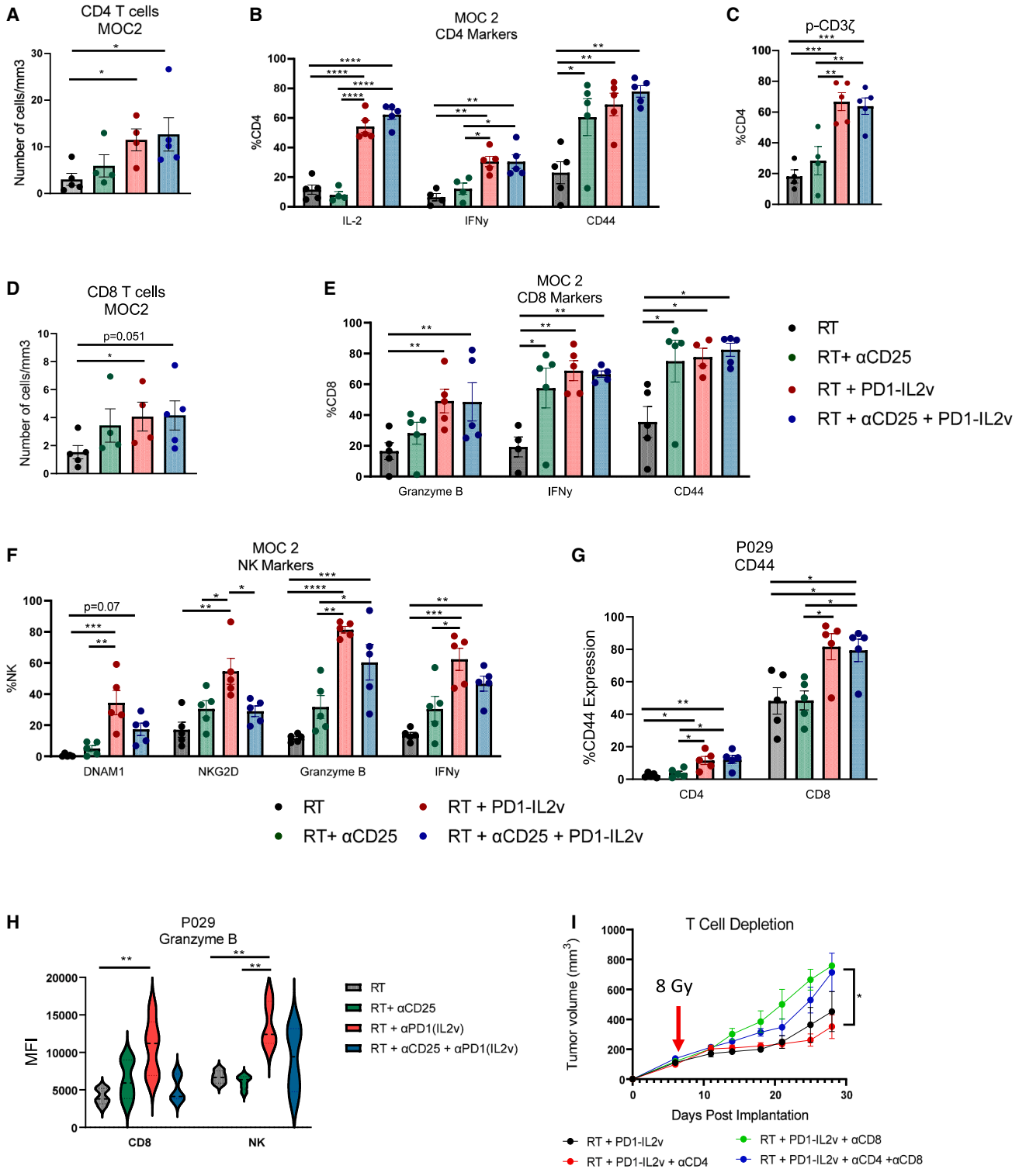

Figure 3. PD1-IL2v alters the composition of the TME

(A) Abundance of CD4 T cells in the tumor of MOC2-tumor-bearing mice. Tumors were treated with RT and combination αCD25, PD1-IL2v, or αCD25 and PD1-IL2v and harvested 5 days after final fraction of RT.

(B) Expression IL-2, IFNγ, and CD44 among CD4 T cells in the tumor.

(C) Frequency of phosphorylated CD3ζ expression in CD4 T cells.

(D) Abundance of CD8 T cells in the tumor.

(legend continued on next page)

effective anti-tumor response, pharmacological depletion of CD8s resulted in accelerated tumor growth (Figures 3I and S2G).

PD1-IL2v drives a robust systemic immune response

Given the substantial effect on lymphocyte infiltration and activation within the TME after treatment with PD1-IL2v and RT, we next sought to understand the effect PD1-IL2v has systemically. Examination of lymphocytes taken from the blood of MOC2-tumor-bearing mice revealed a dramatic shift in the frequency and diversity of T cell and NK cell populations (Figures 4A and S3A). Both CD4 and CD8 T cells displayed enhanced activation and proliferation, as evidenced by expression of CD44, IFNγ, granzyme B, LFA-1, and Ki-67 (Figures 4B–4D). Additionally, increased p-STAT5, a downstream transcription factor in the IL-2 signaling pathway, demonstrated the potency of PD1-IL2v in activating signaling via IL-2Rβγ on effectors (Figure S3B).

The effect on T cell populations in mice bearing P029 tumors after treatment with PD1-IL2v was consistent with the MOC2 model (Figures 4E and S3C), with both CD4 and CD8 T cell populations displaying increased effector function and proliferation, denoted by CD44, IFNγ, and Ki-67, respectively (Figures 4F and 4G). Systemic levels of IL-2, IFNγ, and tumor necrosis factor (TNF) all significantly increased upon treatment with PD1-IL2v, coinciding with a trending decrease in IL-10 (Figures S3D and S3E), signifying a systemic shift toward a pro-inflammatory immune response and decreased levels of tolerance. Interestingly, while αCD25 effectively depletes $CD25^+$ Tregs (Figure S3F), we observed an increase in circulating $CD25^-$ $Foxp3^+$ regulatory T cells (Figure S3G). These Tregs, however, also displayed elevated secretion of IFNγ (Figure S3H). Of note, circulating immune populations treated with αPD-1 and DP47-IL2v increased the frequency of both CD8 T cells and Tregs, alongside significantly increased IL-10 production by Tregs (Figures S3I and S3J). These data provide further evidence that the combined actions of RT and IL-2Rβγ agonism specifically on $PD\text{-}1^+$ cells are critical for superior therapeutic effect,[33] with removal of either arm being detrimental to overall survival.

The first step in the development of systemic anti-tumor immunity is represented by antigen presentation and T cell priming in the tumor-draining lymph nodes (dLNs).[41] Consistent with their intratumoral and circulating counterparts, we observed similar trends in immune activation in the dLNs in both P029 and MOC2 tumor models. Analysis of dLNs from tumor-bearing mice revealed extensive activation of CD4 and CD8 T cells (Figures 4H–4L and S4A). The increased abundance of cDC1 dendritic cells which directly influence the magnitude of CD8 T cell responses (Figure 4M), alongside elevated phosphorylated-ZAP70 (Figure S4B), suggests improved antigen presentation and TCR engagement, hallmarks of an antigen-specific immune response.[38] Although $Foxp3^+$ Tregs were present at higher frequencies in the dLNs they once again expressed IFNγ when exposed to PD1-IL2v, further hinting at dysregulation (Figures S4C and S4D). Taken together, these data describe the potent potential of PD1-IL2v to induce robust multi-compartmental immunity when used in combination with RT.

Radiation therapy and PD1-IL2v reduces lung metastasis

Owing to the predilection of widespread metastasis in the P029 tumor model and given the increased systemic activation of circulating lymphocytes, we investigated the functional implication of increased immunity on systemic tumor spread. We examined lung tissue collected from orthotopically implanted P029 tumors, harvested at the time of sacrifice (Figure 5A). Groups receiving PD1-IL2v had reduced incidence of lung metastases (Figures 5B and 5C). H&E staining was performed to check for microlesions within lung tissue and, consistent with gross examination, revealed reduced overall presence of lung metastases in the groups receiving PD1-IL2v (Figure 5D). Examination of lungs harvested from αPD-1 and DP47-IL2v treatment groups showed no additional benefit in reducing metastasis when compared to RT alone. As before, RT + αPD-1 + DP47-IL2v appeared unfavorable, with a proportionally higher number of mice exhibiting lung metastases compared to RT alone (Figure S5A). Cancer cells which break off from the primary tumor can enter circulation seed tumors at distant sites.[24] Analysis of circulating tumor cells (CTCs) showed that the percentage of $CD45^-$ cells expressing EpCAM and cytokeratin, both markers of CTCs, were significantly reduced in the groups receiving PD1-IL2v in contrast to RT alone and RT + αCD25 monotherapy (Figures 5E, S5B, and S5C). These data suggest that PD1-IL2v assists in preventing metastatic spread and formation of distant lesions by decreasing the amount of tumor cells in circulation, even in the context of local tumor progression.

Enhanced NK activity correlates with diminished metastatic spread

With the understanding that PD1-IL2v is linked to a reduction in lung metastasis, we next sought to evaluate potential target cells which function to reduce lung metastasis when activated by PD1-IL2v. NK cells have an established role in the immunosurveillance of CTCs in various pre-clinical tumor models,[22,42] and the observed activation of NKs within the TME made them a likely target.

When treated with RT and PD1-IL2v, we observed a significant increase in total NK frequency and absolute counts in the blood

(E) Expression of granzyme B, IFNγ, and CD44 among CD8 T cells in the tumor.
(F) Expression levels of DNAM-1, NKG2D, granzyme B, and IFNγ in NK cell populations in the tumor.
(G) Frequency of CD44 expressed on CD4 and CD8 T cells from P029-tumor-bearing mice.
(H) Expression of granzyme B in CD8 and NK cell of P029-tumor-bearing mice.
(I) Tumor growth curves of P029 tumors treated with RT and PD1-IL2v, with a combination of aCD4 and/or aCD8 to deplete CD4 and CD8 T cells, respectively. Tumors were established in C57bl/6 mice and treated with 8 Gy RT at day 7 post implantation. PD1-IL2v was administered weekly via i.p. injection, aCD4 and aCD8 were administered twice weekly via i.p. injection.
One-way ANOVA was used for statistical analysis unless stated otherwise. n = 5–7. Data are presented as mean ± SEM. *$p < 0.05$, **$p < 0.005$, ***$p < 0.0005$, ****$p < 0.0001$.

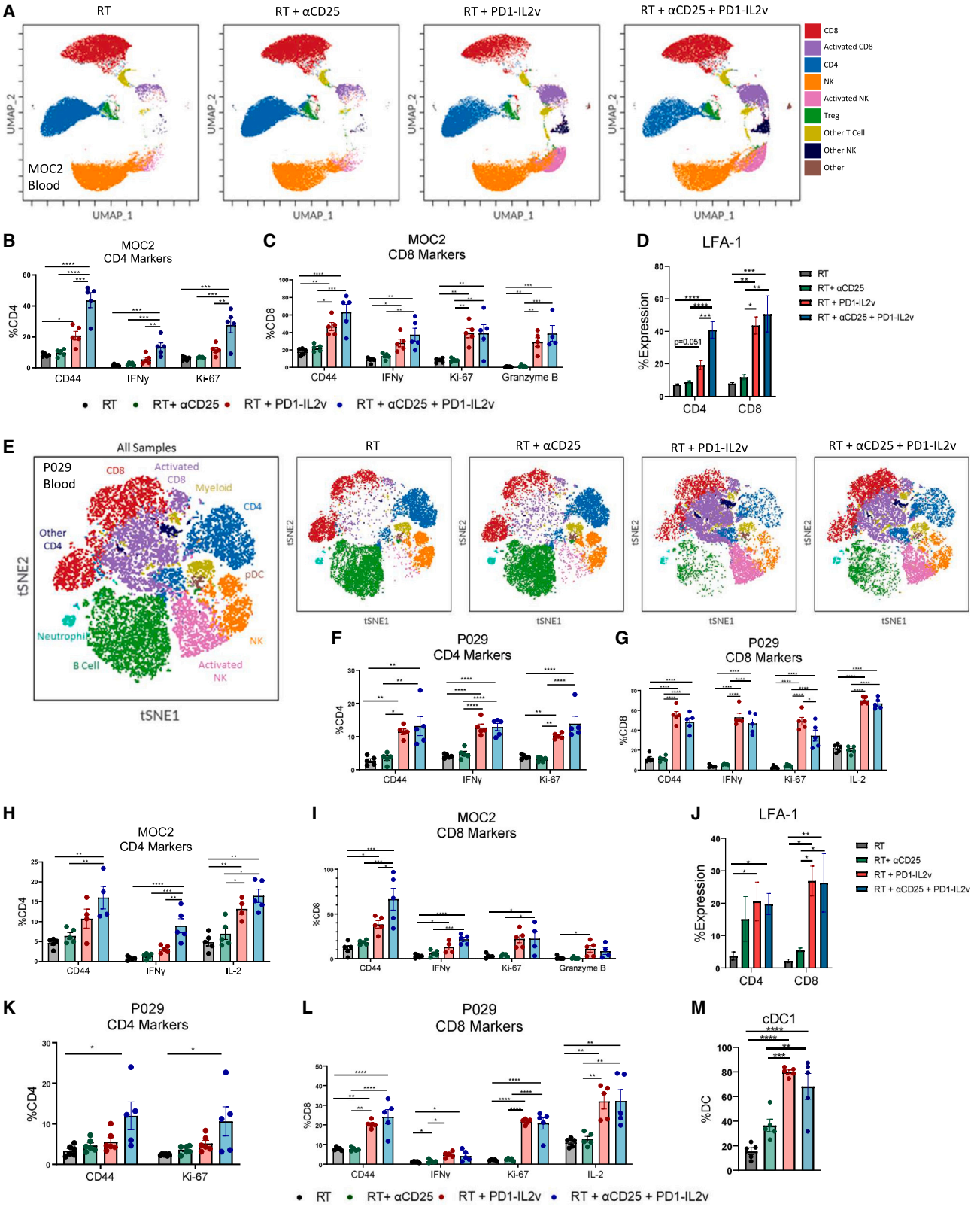

(legend on next page)

(Figures 6A and S6A). Circulating NK cells exhibited significantly increased activation in both P029 and MOC2 tumor models. In the presence of PD1-IL2v, NKs display improved effector and proliferative function, with increases in granzyme B, IFNγ, and Ki-67, along with the activating receptor DNAM-1, downregulation of which negatively impacts metastatic burden[43] (Figures 6B and 6C). Furthermore, surface expression of LFA-1, which helps improve cytotoxicity by strengthening the immunological synapse, and NKG2D, another activating receptor of crucial importance in detecting aberrant cells, are both significantly increased by PD1-IL2v[22,44] (Figure 6D). Interestingly, a cluster of $CD8^+$ NK cells was identified after treatment with PD1-IL2v (Figures S6B and S6C). These NK cells have been previously described in the literature as a highly cytotoxic, polyfunctional subpopulation and are associated with delayed disease progression in chronic HIV-1 infection.[45,46]

Unbiased clustering of peripheral NK cells revealed a phenotypic shift from resting inactive NKs to highly active, cytotoxic NKs (Figures 6D and S6D). These data point to NK cells as playing a critical role in controlling the spread of metastasis, and we hypothesized that depletion of NK cells would accelerate metastasis even in the presence of PD1-IL2v. To test this hypothesis, P029 tumors were established and treated with PD1-IL2v, with or without NK cell depletion. Pharmacological depletion of NK cells using αNK1.1 had minimal impact on local tumor growth but resulted in increased frequency of CTCs (Figures 6F and S6E–S6G). Assessment of lung histology confirmed that ablation of NK cells removes the beneficial effect of PD1-IL2v on the development of lung metastases, with NK-cell-depleted mice showing significantly higher tumor burden in the lung (Figures 6G and S6H–S6J).

CD8 T cells and NK cells undergo functional changes in response to PD1-IL2v

Given that both CD8 T cells and NK cells were significantly activated by PD1-IL2v, we wished to better understand the large-scale effects of PD1-IL2v on these populations. Proteomic analyses revealed that PD1-IL2v had a significant impact on the NK and CD8 T cell proteomes (Figures 7A, S7A, and S7B). CD8 T cells showed significant increases in the TCR signaling components CD3ζ and ZAP70 (Figure 7B), which is consistent with the increased phosphorylated CD3ζ and ZAP70 observed earlier. Likewise, TCF1 showed a marked increase in groups receiving PD1-IL2v, denoting a population of stem-like, antigen experienced CD8 T cells[33] (Figure S7C).

Cellular metabolism governs the functional state of NK cells, and changes in metabolic processes are closely tied to their cytotoxic activity.[47,48] IL-2 signaling in NK cells increases glycolysis and oxidative phosphorylation, prominent processes that are important for production of IFN-γ and granzyme B.[47–49] Key metabolic enzymes of glycolysis (glyceraldehyde 3-phosphate dehydrogenase, lactate dehydrogenase A [LDHA]) and the Krebs cycle (succinate dehydrogenase [SDHA]) were found to be significantly upregulated in NK cells following PD1-IL2v treatment (Figure 7C).

PD1-IL2v drives an enrichment of NK-activating receptors, augmenting metastatic tumor cell kill

NK cell cytotoxicity is regulated by a series of activating and inhibitory receptors that integrate the expression of ligands on the target cell surface.[13,22,50,51] An increase in expression of activating receptors can provide the necessary signals for NK cells to exert their cytotoxic potential on tumor cells.[52–54] Therefore, we wished to understand how the repertoire of activating receptors on the NK cell surface changes during treatment. NK cells display increased activating receptor diversity upon treatment with PD1-IL2v (Figure 7D). To functionally assess whether PD1-IL2v-stimulated NK cells are more cytotoxic, we conducted an *in vitro* cytotoxicity assay[55] to assess NK cell capacity for cytotoxic cell kill. Isolated NK cells treated with PD1-IL2v *in vivo* showed significantly higher tumor-cell-directed cytotoxicity when compared to NK cells from untreated control mice (Figure 7E), a process visualized by employing the use of Imagestream cytometric analysis (Figure 7F). Taken together, these data show that PD1-IL2v alters the proteomic landscape of NK cells, enhancing the utilization of numerous metabolic pathways, and upregulating the expression and diversity of activating receptors on the NK cell surface. These altered cellular dynamics increase NK cell cytotoxic potential, ultimately enhancing the clearance of CTCs.

Figure 4. PD1-IL2v induces robust systemic immune activation

(A) Uniform manifold approximation and projection plots of circulating lymphocytes in mice with established MOC2 tumors (n = 5). Treatment was carried out as described in Figure 3.

(B) Analysis of CD44, IFNγ, and Ki-67 expression in CD4 T cells.

(C) Expression of CD44, IFNγ, Ki-67, and granzyme B in CD8 T cells.

(D) LFA-1 expression in CD4 and CD8 T cells among treatment groups.

(E) Visual stochastic neighbor embedding (viSNE) analysis of immune cell clusters from blood of P029-tumor-bearing mice, treated with combination RT and αCD25, PD1-IL2v, or αCD25 and PD1-IL2v. Blood was harvested, and flow cytometry was performed 4 days after final fraction of RT. RT was delivered as three fractions of 8 Gy. All samples combined (left panel); combined samples from individual groups (right panels).

(F and G) Flow-cytometric analysis of activation markers in (F) CD4 and (G) CD8 immune populations in the blood of P029-tumor-bearing mice.

(H) Expression of CD44, IFNγ, and IL-2 in CD4 T cells in the tumor-draining lymph node of MOC2-tumor-bearing mice.

(I) Expression of CD44, IFNγ, Ki-67, and granzyme B in CD8 T cells in the tumor-draining lymph node of MOC2-tumor-bearing mice.

(J) LFA-1 expression in CD4 and CD8 T cell populations in the tumor-draining lymph nodes.

(K) Expression of CD44 and Ki-67 on CD4 T cells in the tumor-draining lymph nodes of P029-tumor-bearing mice.

(L) Expression of CD44, IFNγ, Ki-67, and IL-2 in the tumor-draining lymph node of P029-tumor-bearing mice.

(M) Frequency of cDC1 dendritic cells in the lymph node, defined as $CD3^-$ $CD11c^+$ MHC II^+, $CD8^+$.

Statistical analysis was performed using one-way ANOVA unless stated otherwise. n = 5. Data are presented as mean ± SEM. *$p < 0.05$, **$p < 0.005$, ***$p < 0.0005$, ****$p < 0.0001$.

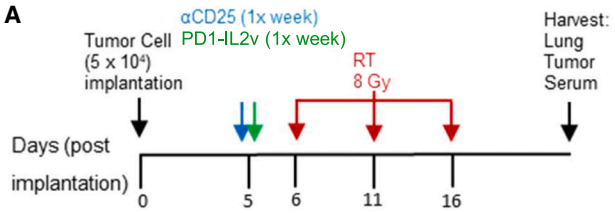

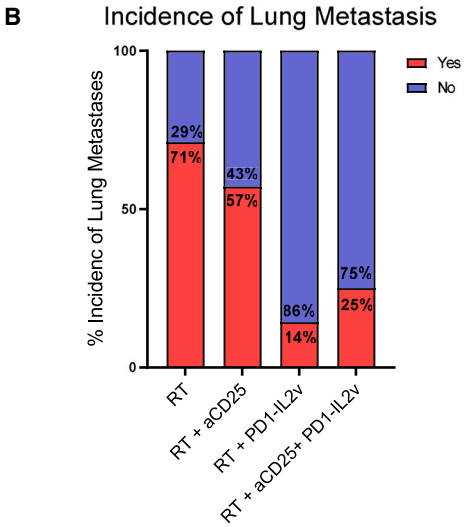

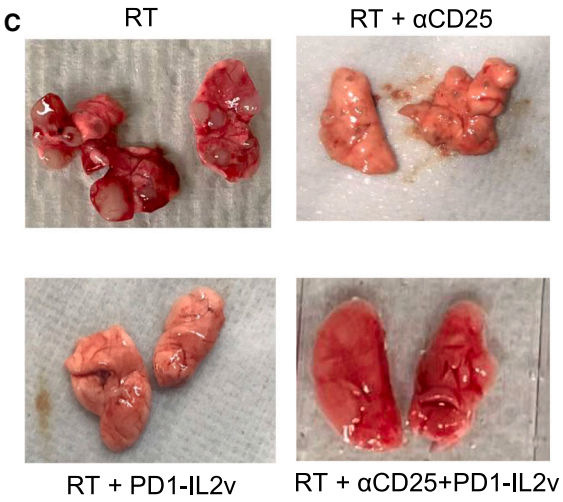

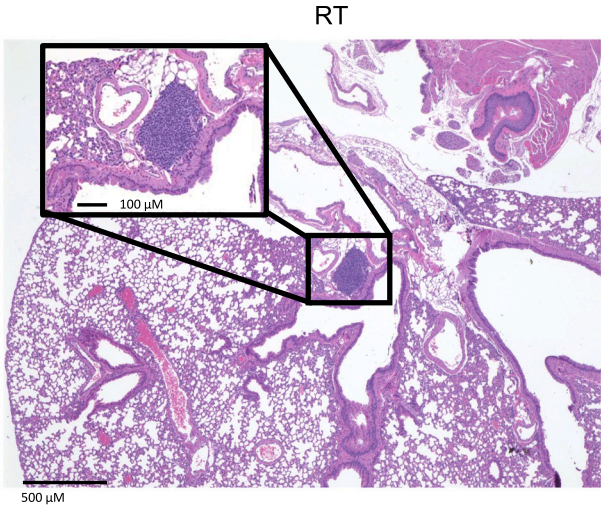

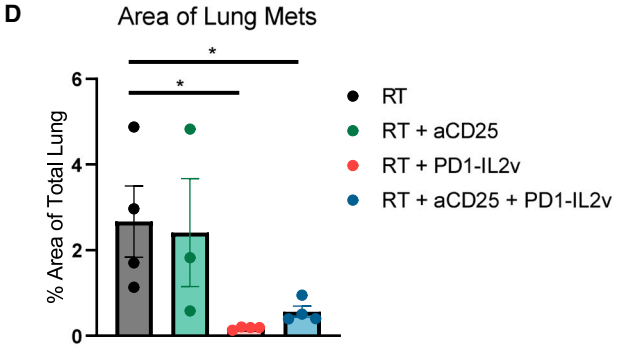

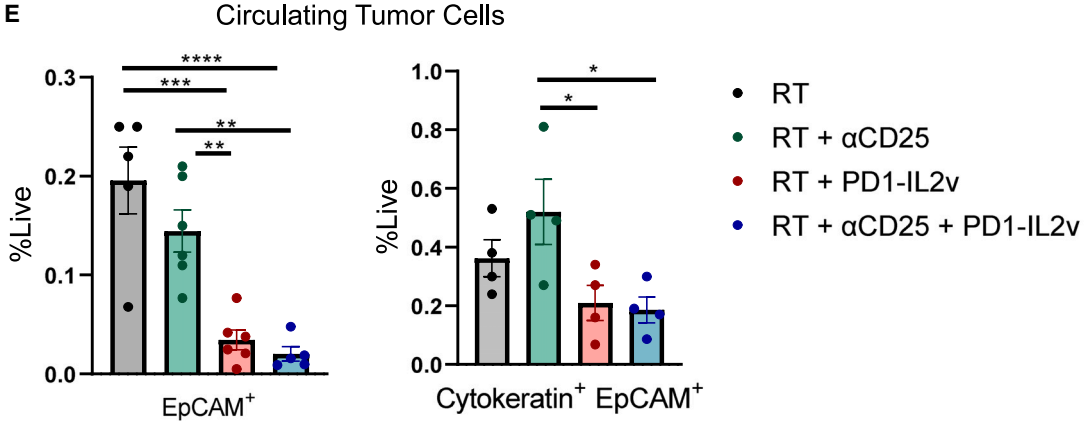

(legend on next page)

DISCUSSION

Despite advancing options in the realm of cancer therapeutics, overall response to immunotherapy in poorly immune infiltrated "cold" tumors remains low.[3] In this work, we investigated the effects of PD1-IL2v in modulating the immune landscape of multiple pre-clinical HNSCC tumor models. We demonstrated that when used in conjunction with RT, PD1-IL2v invigorates CD4 and CD8 T cell immunity across multiple immunologic compartments, promoting infiltration into the TME and generating durable tumor control. We also identified a role for PD1-IL2v in reducing the rate of metastatic spread through the activation of NK cells. Together, these three populations work in concert to control and lower the tumor burden system wide.

IL-2 signaling is a key immune cell regulator, leading to activation and proliferation in NK cells and T cells.[14,27] However, the pleiotropic nature of IL-2 means that it consequently induces activation in immunosuppressive Tregs as well. The unique activity of the IL2v moiety allows PD1-IL2v to specifically target the intermediate-affinity IL-2 receptor IL-2R$\beta\gamma$, bypassing IL-2Rα, which is preferentially expressed on Tregs.[20,33–35] The ability to bypass IL-2Rα and thus negate the activation of Tregs relinquishes IL-2 that under normal circumstances would be consumed by Tregs, making it available for utilization by NK cells and effector T cells.[10,50] However, to maintain immunological tolerance, excessive activation of effector T cells typically results in upregulation of exhaustion markers such a PD-1,[56] blunting responses through progressive loss of T cell function.[57] Using PD1-IL2v was ideal to expand and activate immune effectors by stimulating IL-2 signaling while sustaining function and preventing T cell exhaustion through the blockade of PD-1. Codarri Deak and colleagues describe the induction and expansion of a highly cytotoxic CD8 T cell population upon treatment with PD1-Il2v. This population was demonstrated to have robust effector function in models of chronic viral infection and pancreatic cancer,[20] recapitulating similar qualities we observed in our tumor models.

PD-1 on effector immune cells acts as an immunological "off switch," and blockade of PD-1 can restore effector function. However, Kumagi et al. have reported that interfering with the PD-1/PD-L1 axis can amplify the immunosuppressive capacity of PD-1-expressing Tregs.[18,19] We observed that PD1-IL2v increased the frequency of Foxp3-expressing CD4 T cells. However, PD1-IL2v induced IFNγ production by Tregs and decreased the expression of IL-10, suggestive of Treg fragility. The notion of Treg dysfunction or "fragility" centers on their loss of immunosuppressive functionality while still retaining expression of Foxp3. The underlying mechanisms behind the induction of a fragile Treg phenotype are not fully understood, yet it appears that the functional state of Tregs is an often overlooked aspect of the responsiveness to immunotherapy.[39] Loss of NRP1 on Tregs was found to be a necessary component of response to αPD-1 therapy in models of colon cancer.[39] This led to production of IFNγ by Tregs and induction of a fragile phenotype with reduced immunosuppressive potential, ultimately rendering the tumors susceptible to therapy.[39] Similarly, our past work has shown that combination radioimmunotherapy can induce a state of Treg fragility to help overcome acquired resistance, reprogramming Tregs from immunosuppressive to cytotoxic.[36] Additionally, a study by Drerup et al. showed that stimulating IL-2 signaling using an IL-2 complex that similarly targets IL-2R$\beta\gamma$ not only yielded improved effector T cell function, but also reduced Treg function by inducing Treg fragility.[58]

Tregs are recognized as a significant barrier in establishing anti-tumor immunity, with higher levels of intratumoral Tregs being a detriment to therapeutic response and correlating with poor prognosis in various cancers.[59–62] The ablation of Tregs is an attractive option to negate the detrimental effects of IL-2 signaling while providing selective activation of effector T cell populations. However, similar to our current findings, and with the exception of the LY2 model, depletion of Tregs has only seen modest success in pre-clinical and clinical settings, casting doubt on its true viability as a treatment option. PC-61, the most commonly used clone of αCD25, does not effectively penetrate the TME, leading to ineffective depletion of intratumoral Tregs.[35,63] While this can be circumvented in pre-clinical models by administering αCD25 prior to or shortly after tumor implantation,[8] this strategy is neither clinically nor biologically relevant. Our findings demonstrate that even with an αCD25 antibody able to deplete tumor-infiltrating Tregs, depletion failed to enhance survival in most models. This emphasizes that PD1-IL2v itself may be sufficient to override the immunosuppressive activity of Tregs.

Although the rate of distant metastasis in HNSCC is relatively low compared to other cancer types, affecting approximately 10%–15% of patients, those presenting with metastasis at the time of diagnosis or who develop metastases as the disease progresses have substantially reduced mortality and overall survival outcome.[64,65] There is extensive literature demonstrating that NK cells play a prominent role in the control of distant metastases and destruction of CTCs. The ability of NK cells to

Figure 5. Radiation therapy and PD1-IL2v abrogates lung metastasis

(A) Schematic describing experimental design. P029 tumors were established in C57Bl/6 mice and treated with RT and a combination of αCD25, PD1-IL2v, αCD25 and PD1-IL2v, or no immunotherapy. RT was delivered as three fractions of 8 Gy RT, 5 days apart. Antibodies were administered weekly via i.p. injection beginning 1 day prior to RT.

(B) Incidence of mice that displayed gross lung metastasis at the time of sacrifice. n = 7–8.

(C) Representative mouse lungs from each treatment group showing the difference in gross lung lesions.

(D) Representative H&E staining and quantification of lungs taken from tumor-bearing P029 mice at the time of sacrifice. Three to four lungs were stained per group.

(E) Frequency of circulating tumor cells (CTCs) in the blood of tumor-bearing P029 mice. CTCs are defined as CD45$^-$ EpCAM$^+$ and CD45$^-$ EpCAM$^+$ pan-cytokeratin$^+$.

Statistical analysis was performed using one-way ANOVA unless stated otherwise. Data are presented as mean ± SEM. *p < 0.05, **p < 0.005, ***p < 0.0005, ****p < 0.0001. Scale bar = 500 μM for 4x image and 100 μM for inset image.

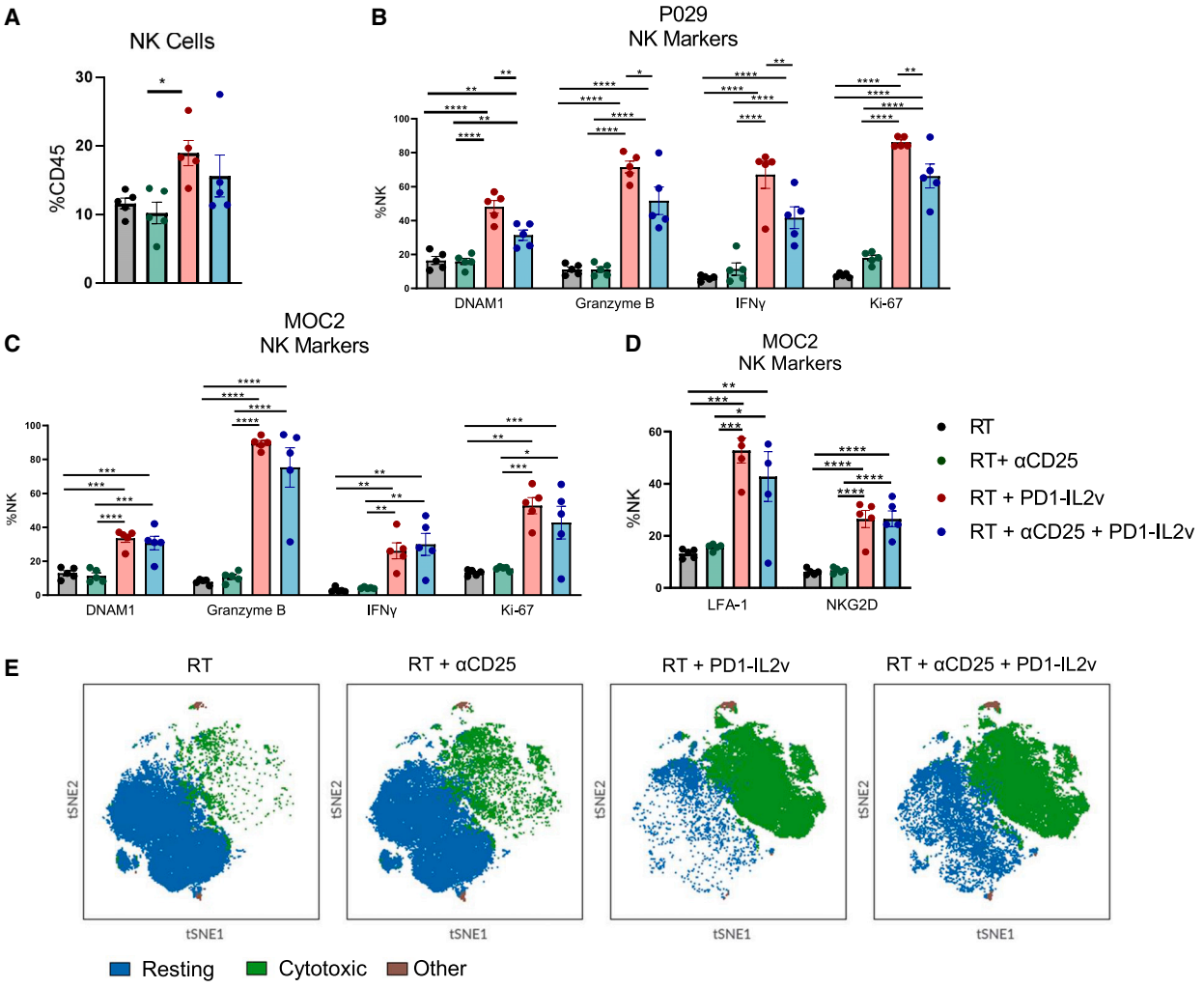

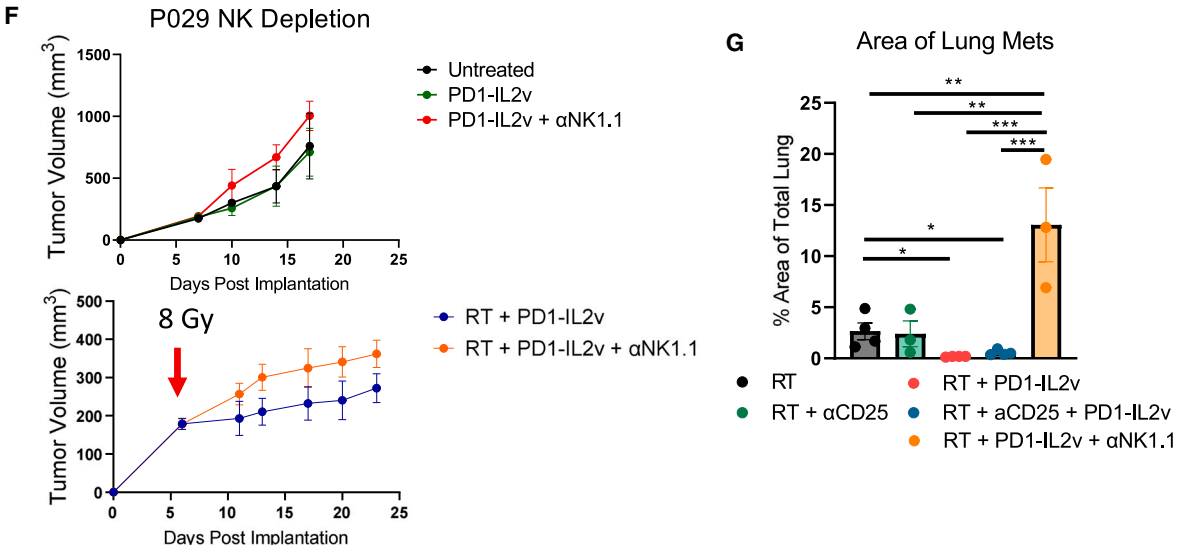

(legend on next page)

discriminate and recognize altered cancerous cells, without prior sensitization, makes them uniquely suited to rapidly eliminate tumor cells in circulation, thereby limiting their ability to disseminate and seed at distant sites.[22,23,42] Upon treatment with PD1-IL2v, we observed significant increases in NK cell activation, proliferation, and cytotoxicity, coinciding with a significant decrease in metastasis to the lungs and frequency of CTCs. These changes coincided with an increased expression and diversity of NK-activating receptors. Previous studies have demonstrated that mice genetically deficient in NKp46, also referred to as NCR1, have an impaired ability to clear metastases in models of metastatic melanoma.[66,67] In contrast, the overexpression of NKp46 on NK cells leads to enhanced clearance of metastatic melanoma lesions,[68] whereas deficiencies in NKG2D lead to increased incidences of prostate cancer and accelerated growth in lymphomas.[69] Clinically, high expression of both NKp46 and NKG2D in the primary tumor is linked to decreased metastasis in patients with prostate carcinomas[70] and underscores the importance of functional NK cells in regulating metastatic disease.

Our proteomic analysis uncovered that PD1-IL2v alters the dynamics of NK metabolism, and the critical role that cellular metabolism plays in helping shape an effective immune response is an underappreciated facet of immunobiology.[47,71] Upon activation, NK cells heavily utilize glycolysis to fuel increased metabolic demands to carry out their effector and cytolytic functions.[71] However, both glycolytic and oxidative phosphorylation pathways are imperative for optimal NK cell function.[47,49,72,73] LDHA, a component of glycolysis, has been shown to support NK cell anti-tumor function and when disrupted NK cells had impaired proliferation, activating receptor signaling, and cytotoxicity.[74] Furthermore, high expression of SDHA acts as a prognostic factor in multiple myeloma, demonstrating the value of monitoring components of metabolic pathways as potential biomarkers.[75]

In summary, our data establish PD1-IL2v as an attractive and promising therapeutic addition to the oncologic armamentarium and support its potential use in combination with RT in the treatment of head and neck cancer, particularly in patients presenting with locoregional or distant metastases.

Limitations of the study

While PD1-IL2v was extensively studied in multiple murine models of the head and neck, this therapy was not tested using human immune cells. IL-2 agonism has historically been accompanied with severe side effects in humans; however, these metrics and adverse events are much more difficult to assess in mouse models than they are in human patients. Furthermore, the use of syngeneic mouse models does not accurately mimic the natural heterogeneity of clinical tumors.

STAR★METHODS

Detailed methods are provided in the online version of this paper and include the following:

- KEY RESOURCES TABLE
- RESOURCE AVAILABILITY
  - Lead contact
  - Materials availability
  - Data and code availability
- EXPERIMENTAL MODEL AND SUBJECT PARTICIPANT DETAILS
  - Cell lines
  - Mouse models
  - Tumor studies
  - Human patient samples
- METHOD DETAILS
  - Antibodies and drugs
  - Irradiation
  - Flow cytometry
  - Immunohistochemistry and H&E staining
  - Human pathways analysis and mass cytometry analysis
  - NK cytotoxicity assay
  - Imagestream cytometry
  - Proteomics
  - Human single cell RNA sequencing analysis
  - Dimensionality reduction algorithms and self organized mapping
  - Cytokine quantification
- QUANTIFICATION AND STATISTICAL ANALYSIS
- ADDITIONAL RESOURCES

SUPPLEMENTAL INFORMATION

Supplemental information can be found online at https://doi.org/10.1016/j.xcrm.2023.101150.

Figure 6. PD1-IL2v decreases metastasis by enhancing NK-mediated immune surveillance

(A) Frequency of NK cells in blood of P029-tumor-bearing mice treated with combination RT and αCD25, PD1-IL2v, or αCD25 and PD1-IL2v. Blood was harvested, and flow cytometry was performed 4 days after final fraction of RT. RT was delivered as three fractions of 8 Gy.

(B) Expression of NK cell activation markers DNAM-1, granzyme B, IFNγ, and Ki-67 from P029-tumor-bearing mice across treatment groups.

(C) Expression of NK cell activation markers DNAM-1, granzyme B, IFNγ, and Ki-67 from MOC2-tumor-bearing mice across treatment groups.

(D) Expression of LFA-1 and NKG2D on NK cells of MOC2-tumor-bearing mice across treatment groups.

(E) viSNE analysis and FlowSOM clustering of circulating NK cells among different treatment groups.

(F) Tumor growth curves of P029 tumors treated with PD1-IL2v, with or without NK cell depletion and with or without RT. Tumors were established in C57bl/6 mice and treated with 8 Gy RT at day 7 post implantation. PD1-IL2v was administered weekly via i.p. injection, and αNK1.1 was administered twice weekly via i.p. injection to deplete NK cells. NK cell depletion was verified via flow cytometry.

(F) Representative lungs from groups treated with RT and PD1-IL2v with and without NK cell depletion.

(G) Quantification of H&E staining showing the percentage of total that is tumor. Three to four were stained per group.

Statistical analysis was performed using one-way ANOVA unless stated otherwise. Data are presented as mean ± SEM. *$p < 0.05$, **$p < 0.005$, ***$p < 0.0005$, ****$p < 0.0001$.

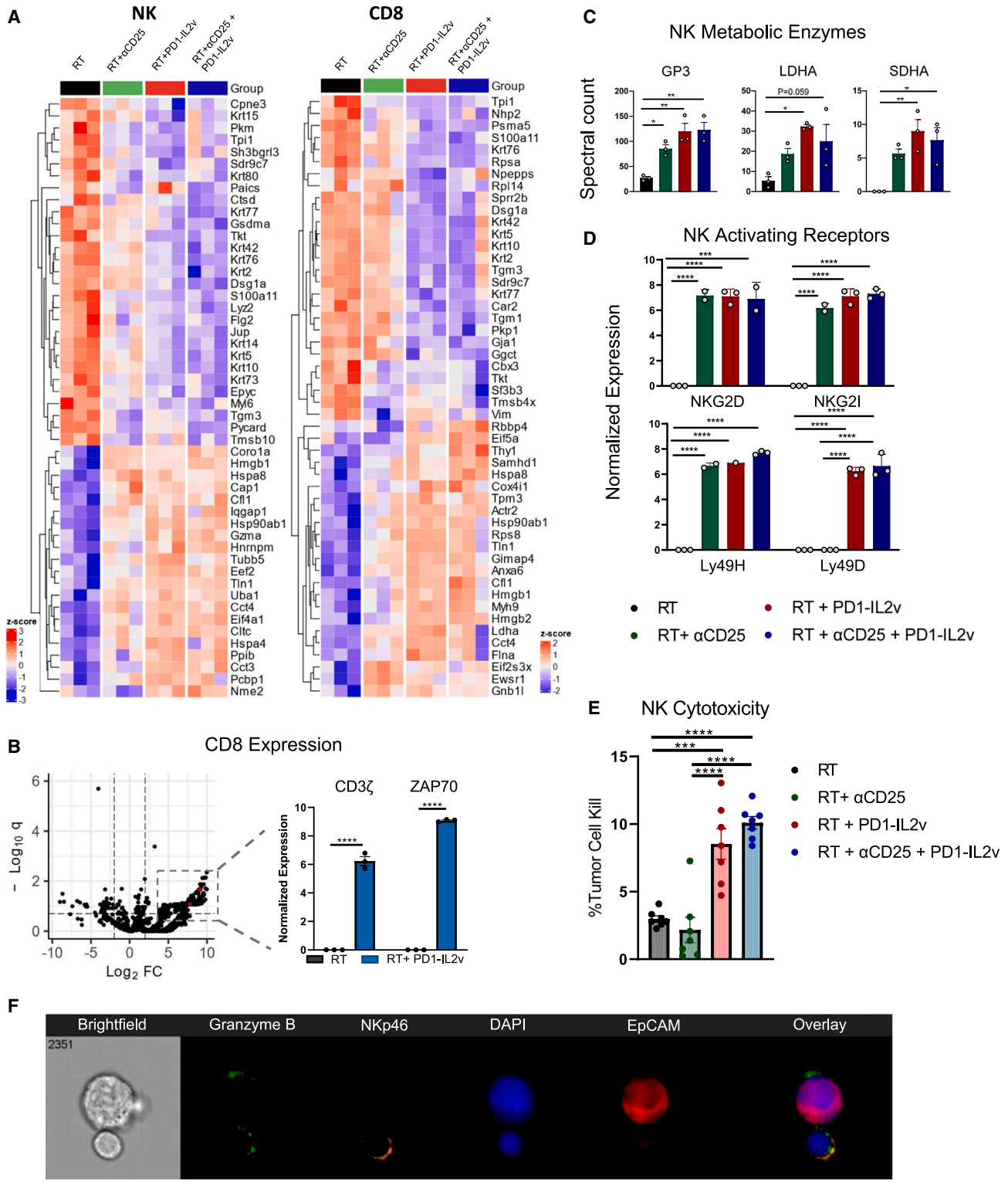

Figure 7. CD8 T cells and NK cells undergo functional changes in response to PD1-IL2v

(A) Heatmaps of NK and CD8 T cells showing the top 75 most expressed proteins. Tumors were established in C57Bl/6 mice and treated with RT and combination of αCD25, PD1-IL2v, αCD25 and PD1-IL2v, or no immunotherapy. Tumors were treated with three fractions of 8 Gy RT given 5 days apart. Antibodies were administered 1 day prior to beginning RT. Tumors were harvested 4 days after the final dose of RT, and NK cells were isolated using NK cell isolation kit and cell sorting. n = 3.

(legend continued on next page)

ACKNOWLEDGMENTS

S.D.K. receives funding from the NIDCR/NCI (R01 DE028528-01; R01 DE028282-01; R01 CA284561-01; 1 P50 CA261605-01) and clinical trial funding from AstraZeneca, Genentech, and Ionis, all of which are unrelated to this work. S.D.K reports partial grant funding of this project by Roche, all in direct costs for research. We would like to thank the remaining members of the Karam lab for their technical support throughout this study. We also thank the Barbara Davis Center Cell and Tissue Analysis Core (NIDDK P30-DK116073) for support and access to flow cytometry resources. Biorender was used to make graphical abstract.

AUTHOR CONTRIBUTIONS

J.G.: conceptualization, experimental design, performed experiments, data analysis, manuscript writing and editing. M.A.: conceptualization, experimental design, and support. T.E.B.: experimental design, data analysis, performed experiments, manuscript editing and review. M.W.K.: bioinformatics and RNA sequencing support, data validation, manuscript editing and review. L.B.D.: data validation, technical feedback, manuscript editing and review. M.P.: data validation, manuscript editing and review. B.V.C.: data validation, manuscript editing and review. S.B.: performed experiments, manuscript editing and review. T.T.P.: manuscript editing and review. X.-J.W.: provided *in vivo* resources, manuscript editing and review. A.J.S.: data validation. L.C.D.: provided reagents, manuscript review. C.K.: provided reagents, manuscript editing and review. P.U.: provided reagents, manuscript review. A.D.: experimental design and support, data validation, manuscript editing and review. S.D.K.: study supervision, conceptualization, experimental design, data validation, manuscript editing and review. All authors contributed and approved submission of the manuscript.

DECLARATION OF INTERESTS

M.A., L.C.D., P.U., and C.K. are employed by Roche Innovation Center Zurich and declare ownership of stock and patents with Roche. S.D.K. receives funding from NIDCR/NCI in addition to clinical trial funding from AstraZeneca, Genentech, and Ionis outside the submitted work. S.D.K. reports no personal payment in consulting, advisory boards, clinical trials, or any other relevant financial disclosures. A.D. is a founder of Omix Technologies Inc. and Altis Biosciences. A.D. is a scientific advisory board member for Hemanext Inc., Macopharma Inc., and Forma Therapeutics.

Received: July 6, 2022
Revised: April 21, 2023
Accepted: July 18, 2023
Published: August 15, 2023

REFERENCES

1. Sambi, M., Bagheri, L., and Szewczuk, M.R. (2019). Current challenges in cancer immunotherapy: multimodal approaches to improve efficacy and patient response rates. J. Oncol. *2019*, 4508794. https://doi.org/10.1155/2019/4508794.
2. Nör, J.E., and Gutkind, J.S. (2018). Head and neck cancer in the new era of precision medicine. J. Dent. Res. *97*, 601–602. https://doi.org/10.1177/0022034518772278.
3. Mandal, R., Şenbabaoğlu, Y., Desrichard, A., Havel, J.J., Dalin, M.G., Riaz, N., Lee, K.W., Ganly, I., Hakimi, A.A., Chan, T.A., and Morris, L.G. (2016). The head and neck cancer immune landscape and its immunotherapeutic implications. JCI Insight *1*, e89829. https://doi.org/10.1172/jci.insight.89829.
4. Karam, S.D., and Raben, D. (2019). Radioimmunotherapy for the treatment of head and neck cancer. Lancet Oncol. *20*, e404–e416. https://doi.org/10.1016/S1470-2045(19)30306-7.
5. Waldman, A.D., Fritz, J.M., and Lenardo, M.J. (2020). A guide to cancer immunotherapy: from T cell basic science to clinical practice. Nat. Rev. Immunol. *20*, 651–668. https://doi.org/10.1038/s41577-020-0306-5.
6. Botticelli, A., Mezi, S., Pomati, G., Cerbelli, B., Di Rocco, C., Amirhassankhani, S., Sirgiovanni, G., Occhipinti, M., Napoli, V., Emiliani, A., et al. (2020). The 5-Ws of immunotherapy in head and neck cancer. Crit. Rev. Oncol. Hematol. *153*, 103041. https://doi.org/10.1016/J.CRITREVONC.2020.103041.
7. Oweida, A., Hararah, M.K., Phan, A., Binder, D., Bhatia, S., Lennon, S., Bukkapatnam, S., Van Court, B., Uyanga, N., Darragh, L., et al. (2018). Resistance to radiotherapy and PD-L1 blockade is mediated by TIM-3 up-regulation and regulatory T-cell infiltration. Clin. Cancer Res. *24*, 5368–5380. https://doi.org/10.1158/1078-0432.CCR-18-1038.
8. Oweida, A.J., Darragh, L., Phan, A., Binder, D., Bhatia, S., Mueller, A., Court, B.V., Milner, D., Raben, D., Woessner, R., et al. (2019). STAT3 modulation of regulatory T cells in response to radiation therapy in head and neck cancer. J. Natl. Cancer Inst. *111*, 1339–1349. https://doi.org/10.1093/jnci/djz036.
9. Ihara, F., Sakurai, D., Horinaka, A., Makita, Y., Fujikawa, A., Sakurai, T., Yamasaki, K., Kunii, N., Motohashi, S., Nakayama, T., and Okamoto, Y. (2017). CD45RA−Foxp3high regulatory T cells have a negative impact on the clinical outcome of head and neck squamous cell carcinoma. Cancer Immunol. Immunother. *66*, 1275–1285. https://doi.org/10.1007/S00262-017-2021-Z.
10. Bickett, T.E., Knitz, M., Darragh, L.B., Bhatia, S., Van Court, B., Gadwa, J., Bhuvane, S., Piper, M., Nguyen, D., Tu, H., et al. (2021). FLT3L release by natural killer cells enhances response to radioimmunotherapy in preclinical models of HNSCC. Clin. Cancer Res. *27*, 6235–6249. https://doi.org/10.1158/1078-0432.ccr-21-0971.
11. Martin, J.F., Perry, J.S.A., Jakhete, N.R., Wang, X., and Bielekova, B. (2010). An IL-2 paradox: blocking CD25 on T cells induces IL-2–driven activation of CD56 bright NK cells. J. Immunol. *185*, 1311–1320. https://doi.org/10.4049/jimmunol.0902238.
12. Gras Navarro, A., Björklund, A.T., and Chekenya, M. (2015). Therapeutic potential and challenges of natural killer cells in treatment of solid tumors. Front. Immunol. *6*, 202. https://doi.org/10.3389/fimmu.2015.00202.
13. Vivier, E., Tomasello, E., Baratin, M., Walzer, T., and Ugolini, S. (2008). Functions of natural killer cells. Nat. Immunol. *9*, 503–510. https://doi.org/10.1038/ni1582.
14. Sim, G.C., and Radvanyi, L. (2014). The IL-2 cytokine family in cancer immunotherapy. Cytokine Growth Factor Rev. *25*, 377–390. https://doi.org/10.1016/J.CYTOGFR.2014.07.018.
15. Wu, Y., Tian, Z., and Wei, H. (2017). Developmental and functional control of natural killer cells by cytokines. Front. Immunol. *8*, 930. https://doi.org/10.3389/fimmu.2017.00930.

(B) Volcano plot of CD8 T cell protein expression of significantly up- or downregulated genes between RT and RT + PD1-IL2v with false discovery rate <0.20. Log_2CPM expression of CD3ζ and ZAP70. Statistical analysis was performed using unpaired two-sided t test.
(C) Proteomic expression of enzymes associated with metabolic pathways from NK cells.
(D) Expression of activating and inhibitory receptors on NK cell surface.
(E) Percent cell kill of P029 tumor cells *in vitro* by harvested NK cells treated with PD1-IL2v vs. untreated. Isolated NK cells were pooled and split into seven technical replicates per treatment condition.
(F) Image stream cytometry analysis of NK cell-tumor cell interaction *in vitro* stimulated with PD1-IL2v showing direct NK-tumor cell contact.
One-way ANOVA was used for all statistical analyses unless stated otherwise. Data are presented as mean ± SEM. *p < 0.05, **p < 0.005, ***p < 0.0005, ****p < 0.0001.

16. Koyama, S., Akbay, E.A., Li, Y.Y., Herter-Sprie, G.S., Buczkowski, K.A., Richards, W.G., Gandhi, L., Redig, A.J., Rodig, S.J., Asahina, H., et al. (2016). Adaptive resistance to therapeutic PD-1 blockade is associated with upregulation of alternative immune checkpoints. Nat. Commun. *7*, 10501. https://doi.org/10.1038/ncomms10501.

17. Sharpe, A.H., and Pauken, K.E. (2018). The diverse functions of the PD1 inhibitory pathway. Nat. Rev. Immunol. *18*, 153–167. https://doi.org/10.1038/nri.2017.108.

18. Kumagai S, Togashi Y, Kamada T, Sugiyama E., Nishinakamura H., Takeuchi Y., Vitaly K., Itahashi K., Maeda Y., Matsui S. et al. The PD-1 expression balance between effector and regulatory T cells predicts the clinical efficacy of PD-1 blockade therapies.Nat. Immunol. 21 1346-1358doi:10.1038/s41590-020-0769-3

19. Kamada, T., Togashi, Y., Tay, C., Ha, D., Sasaki, A., Nakamura, Y., Sato, E., Fukuoka, S., Tada, Y., Tanaka, A., et al. (2019). PD-1+ regulatory T cells amplified by PD-1 blockade promote hyperprogression of cancer. Proc. Natl. Acad. Sci. USA *116*, 9999–10008. https://doi.org/10.1073/PNAS.1822001116/-/DCSUPPLEMENTAL.

20. Umaña P., Deak L.C., Ahmed R., Differentiating PD-1+ Stem-like CD8 T Cells towards Distinct Effectors with Enhanced Therapeutic Potential by an Engineered IL-2 Cis-Targeted to PD-1. doi:10.21203/rs.3.rs-329812/v1

21. Chinen, T., Kannan, A.K., Levine, A.G., Fan, X., Klein, U., Zheng, Y., Gasteiger, G., Feng, Y., Fontenot, J.D., and Rudensky, A.Y. (2016). An essential role for the IL-2 receptor in T reg cell function. Nat. Immunol. *17*, 1322–1333. https://doi.org/10.1038/ni.3540.

22. López-Soto, A., Gonzalez, S., Smyth, M.J., and Galluzzi, L. (2017). Control of metastasis by NK cells. Cancer Cell *32*, 135–154. https://doi.org/10.1016/J.CCELL.2017.06.009.

23. Sharma, P., Kumar, P., and Sharma, R. (2017). Natural killer cells - Their role in tumour immunosurveillance. J. Clin. Diagn. Res. *11*, BE01–BE05. https://doi.org/10.7860/JCDR/2017/26748.10469.

24. Lo, H.C., Xu, Z., Kim, I.S., Pingel, B., Aguirre, S., Kodali, S., Liu, J., Zhang, W., Muscarella, A.M., Hein, S.M., et al. (2020). Resistance to natural killer cell immunosurveillance confers a selective advantage to polyclonal metastasis. Nat. Cancer *1*, 709–722. https://doi.org/10.1038/s43018-020-0068-9.

25. Puram, S.V., Tirosh, I., Parikh, A.S., Patel, A.P., Yizhak, K., Gillespie, S., Rodman, C., Luo, C.L., Mroz, E.A., Emerick, K.S., et al. (2017). Single-cell transcriptomic analysis of primary and metastatic tumor ecosystems in head and neck cancer. Cell *171*, 1611–1624.e24. https://doi.org/10.1016/j.cell.2017.10.044.

26. Cillo, A.R., Kürten, C.H.L., Tabib, T., Qi, Z., Onkar, S., Wang, T., Liu, A., Duvvuri, U., Kim, S., Soose, R.J., et al. (2020). Immune landscape of viral- and carcinogen-driven head and neck cancer. Immunity *52*, 183–199.e9. https://doi.org/10.1016/j.immuni.2019.11.014.

27. Boyman, O., and Sprent, J. (2012). The role of interleukin-2 during homeostasis and activation of the immune system. Nat. Rev. Immunol. *12*, 180–190. https://doi.org/10.1038/nri3156.

28. Zimmer, J., Andrès, E., and Hentges, F. (2008). NK cells and Treg cells: a fascinating dance cheek to cheek. Eur. J. Immunol. *38*, 2942–2945. https://doi.org/10.1002/eji.200838813.

29. Ralainirina N, lie Poli A, Michel T, Poos L., Andrès E., Hentges F., Zimmer J. Control of NK cell functions by CD4 CD25 regulatory T cells. J. Leukoc. Biol. 81 144-153doi:10.1189/jlb.0606409

30. Wang, X., Lupardus, P., Laporte, S.L., and Garcia, K.C. (2009). Structural biology of shared cytokine receptors. Annu. Rev. Immunol. *27*, 29–60. https://doi.org/10.1146/annurev.immunol.24.021605.090616.

31. Darragh, L.B., Knitz, M.M., Hu, J., Clambey, E.T., Backus, J., Dumit, A., Samedi, V., Bubak, A., Greene, C., Waxweiler, T., et al. (2022). A phase I/Ib trial and biological correlate analysis of neoadjuvant SBRT with single-dose durvalumab in HPV-unrelated locally advanced HNSCC. Nat. Cancer *3*, 1300–1317. https://doi.org/10.1038/s43018-022-00450-6.

32. Ben-Shmuel, A., Biber, G., and Barda-Saad, M. (2020). Unleashing natural killer cells in the tumor microenvironment–the next generation of immunotherapy? Front. Immunol. *11*, 275. https://doi.org/10.3389/fimmu.2020.00275.

33. Waldhauer, I., Gonzalez-Nicolini, V., Freimoser-Grundschober, A., Nayak, T.K., Fahrni, L., Hosse, R.J., Gerrits, D., Geven, E.J.W., Sam, J., Lang, S., et al. (2021). Simlukafusp alfa (FAP-IL2v) immunocytokine is a versatile combination partner for cancer immunotherapy. mAbs *13*, 1913791. https://doi.org/10.1080/19420862.2021.1913791.

34. Klein, C., Waldhauer, I., Nicolini, V.G., Freimoser-Grundschober, A., Nayak, T., Vugts, D.J., Dunn, C., Bolijn, M., Benz, J., Stihle, M., et al. (2017). Cergutuzumab amunaleukin (CEA-IL2v), a CEA-targeted IL-2 variant-based immunocytokine for combination cancer immunotherapy: overcoming limitations of aldesleukin and conventional IL-2-based immunocytokines. Oncoimmunology *6*, e1277306. https://doi.org/10.1080/2162402X.2016.1277306.

35. Solomon, I., Amann, M., Goubier, A., Arce Vargas, F., Zervas, D., Qing, C., Henry, J.Y., Ghorani, E., Akarca, A.U., Marafioti, T., et al. (2020). CD25-Treg-depleting antibodies preserving IL-2 signaling on effector T cells enhance effector activation and antitumor immunity. Nat. Cancer *1*, 1153–1166. https://doi.org/10.1038/s43018-020-00133-0.

36. Knitz, M.W., Bickett, T.E., Darragh, L.B., Oweida, A.J., Bhatia, S., Van Court, B., Bhuvane, S., Piper, M., Gadwa, J., Mueller, A.C., et al. (2021). Targeting resistance to radiation-immunotherapy in cold HNSCCs by modulating the Treg-dendritic cell axis. J. Immunother. Cancer *9*, e001955. https://doi.org/10.1136/jitc-2020-001955.

37. Gérard, A., Cope, A.P., Kemper, C., Alon, R., and Köchl, R. (2021). LFA-1 in T cell priming, differentiation, and effector functions. Trends Immunol. *42*, 706–722. https://doi.org/10.1016/j.it.2021.06.004.

38. Hwang, J.R., Byeon, Y., Kim, D., and Park, S.G. (2020). Recent insights of T cell receptor-mediated signaling pathways for T cell activation and development. Exp. Mol. Med. *52*, 750–761. https://doi.org/10.1038/s12276-020-0435-8.

39. Overacre-Delgoffe, A.E., Chikina, M., Dadey, R.E., Yano, H., Brunazzi, E.A., Shayan, G., Horne, W., Moskovitz, J.M., Kolls, J.K., Sander, C., et al. (2017). Interferon-γ drives treg fragility to promote anti-tumor immunity. Cell *169*, 1130–1141.e11. https://doi.org/10.1016/J.CELL.2017.05.005.

40. Overacre-Delgoffe, A.E., and Vignali, D.A.A. (2018). Treg fragility: a prerequisite for effective antitumor immunity? Cancer Immunol. Res. *6*, 882–887. https://doi.org/10.1158/2326-6066.CIR-18-0066.

41. Mempel, T.R., Henrickson, S.E., and Von Andrian, U.H. (2004). T-cell priming by dendritic cells in lymph nodes occurs in three distinct phases. Nature *427*, 154–159. www.nature.com/nature.

42. Nakamura, K., and Smyth, M.J. (2020). Immunoediting of cancer metastasis by NK cells. Nat. Cancer *1*, 670–671. https://doi.org/10.1038/s43018-020-0081-z.

43. Briukhovetska, D., Suarez-Gosalvez, J., Voigt, C., Markota, A., Giannou, A.D., Schübel, M., Jobst, J., Zhang, T., Dörr, J., Märkl, F., et al. (2023). T cell-derived interleukin-22 drives the expression of CD155 by cancer cells to suppress NK cell function and promote metastasis. Immunity *56*, 143–161.e11. https://doi.org/10.1016/j.immuni.2022.12.010.

44. Mace, E.M., Zhang, J., Siminovitch, K.A., and Takei, F. (2010). Elucidation of the integrin LFA-1-mediated signaling pathway of actin polarization in natural killer cells. Blood *116*, 1272–1279. https://doi.org/10.1182/blood-2009-12-261487.

45. Addison, E.G., North, J., Bakhsh, I., Marden, C., Haq, S., Al-Sarraj, S., Malayeri, R., Wickremasinghe, R.G., Davies, J.K., and Lowdell, M.W. (2005). Ligation of CD8α on human natural killer cells prevents activation-induced apoptosis and enhances cytolytic activity. Immunology *116*, 354–361. https://doi.org/10.1111/j.1365-2567.2005.02235.x.

46. Ahmad, F., Hong, H.S., Jäckel, M., Jablonka, A., Lu, I.N., Bhatnagar, N., Eberhard, J.M., Bollmann, B.A., Ballmaier, M., Zielinska-Skowronek, M., et al. (2014). High frequencies of polyfunctional CD8 + NK cells in chronic HIV-1 infection are associated with slower disease progression. J. Virol. *88*, 12397–12408. https://doi.org/10.1128/jvi.01420-14.

47. Cong, J. (2020). Metabolism of natural killer cells and other innate lymphoid cells. Front. Immunol. *11*, 1989. https://doi.org/10.3389/fimmu.2020.01989.

48. O'Brien, K.L., and Finlay, D.K. (2019). Immunometabolism and natural killer cell responses. Nat. Rev. Immunol. *19*, 282–290. https://doi.org/10.1038/s41577-019-0139-2.

49. Choi, C., and Finlay, D.K. (2021). Optimising NK cell metabolism to increase the efficacy of cancer immunotherapy. Stem Cell Res. Ther. *12*, 320. https://doi.org/10.1186/s13287-021-02377-8.

50. Waldhauer, I., and Steinle, A. (2008). NK cells and cancer immunosurveillance. Oncogene *27*, 5932–5943. https://doi.org/10.1038/onc.2008.267.

51. Paul, S., and Lal, G. (2017). The molecular mechanism of natural killer cells function and its importance in cancer immunotherapy. Front. Immunol. *8*, 1124. https://doi.org/10.3389/fimmu.2017.01124.

52. Fiegler, N., Textor, S., Arnold, A., Rölle, A., Oehme, I., Breuhahn, K., Moldenhauer, G., Witzens-Harig, M., and Cerwenka, A. (2013). Downregulation of the activating NKp30 ligand B7-H6 by HDAC inhibitors impairs tumor cell recognition by NK cells. Blood, 684–693. https://doi.org/10.1182/blood-2013-02.

53. López-Soto, A., Huergo-Zapico, L., Acebes-Huerta, A., Villa-Alvarez, M., and Gonzalez, S. (2015). NKG2D signaling in cancer immunosurveillance. Int. J. Cancer *136*, 1741–1750. https://doi.org/10.1002/ijc.28775.

54. Duan, S., Guo, W., Xu, Z., He, Y., Liang, C., Mo, Y., Wang, Y., Xiong, F., Guo, C., Li, Y., et al. (2019). Natural killer group 2D receptor and its ligands in cancer immune escape. Mol. Cancer *18*, 29. https://doi.org/10.1186/s12943-019-0956-8.

55. Somanchi, S.S., McCulley, K.J., Somanchi, A., Chan, L.L., and Lee, D.A. (2015). A novel method for assessment of natural killer cell cytotoxicity using image cytometry. PLoS One *10*, e0141074. https://doi.org/10.1371/journal.pone.0141074.

56. Nishimura, H., Nose, M., Hiai, H., Minato, N., and Honjo, T. (1999). Development of lupus-like autoimmune diseases by disruption of the PD-1 gene encoding an ITIM motif-carrying immunoreceptor. Immunity *11*, 141–151. https://doi.org/10.1016/S1074-7613(00)80089-8.

57. Simon, S., and Labarriere, N. (2017). PD-1 expression on tumor-specific T cells: friend or foe for immunotherapy? Oncoimmunology *7*, e1364828. https://doi.org/10.1080/2162402X.2017.1364828.

58. Drerup, J.M., Deng, Y., Pandeswara, S.L., Padrón, Á.S., Reyes, R.M., Zhang, X., Mendez, J., Liu, A., Clark, C.A., Chen, W., et al. (2020). CD122-Selective IL2 Complexes Reduce Immunosuppression, Promote Treg Fragility, and Sensitize Tumor Response to PD-L1 Blockade. Cancer Res *80*, 5063–5075.

59. Miller, A.M., Lundberg, K., Özenci, V., Banham, A.H., Hellström, M., Egevad, L., and Pisa, P. (2006). CD4 + CD25 high T cells are enriched in the tumor and peripheral blood of prostate cancer patients. J. Immunol. *177*, 7398–7405. https://doi.org/10.4049/jimmunol.177.10.7398.

60. Takenaka, M., Seki, N., Toh, U., Hattori, S., Kawahara, A., Yamaguchi, T., Koura, K., Takahashi, R., Otsuka, H., Takahashi, H., et al. (2013). FOXP3 expression in tumor cells and tumor-infiltrating lymphocytes is associated with breast cancer prognosis. Mol. Clin. Oncol. *1*, 625–632. https://doi.org/10.3892/mco.2013.107.

61. O'callaghan, D.S., Rexhepaj, E., Gately, K., Coate, L., Delaney, D., O'Donnell, D.M., Kay, E., O'Connell, F., Gallagher, W.M., and O'Byrne, K.J. (2015). Tumour islet Foxp3 + T-cell infiltration predicts poor outcome in nonsmall cell lung cancer. Eur. Respir. J. *46*, 1762–1772. https://doi.org/10.1183/09031936.00159515.

62. Sun D-S, M.-Q. Zhao, Xia M, Li L., Jiang L Y-H. The correlation between tumor-infiltrating Foxp3+ regulatory T cells and cyclooxygenase-2 expression and their association with recurrence in resected head and neck cancers. Med. Oncol. 29 707-713doi:10.1007/s12032-011-9903-2

63. Arce Vargas, F., Furness, A.J.S., Solomon, I., Joshi, K., Mekkaoui, L., Lesko, M.H., Miranda Rota, E., Dahan, R., Georgiou, A., Sledzinska, A., et al. (2017). Fc-optimized Anti-CD25 depletes tumor-infiltrating regulatory T cells and synergizes with PD-1 blockade to eradicate established tumors. Immunity *46*, 577–586. https://doi.org/10.1016/J.IMMUNI.2017.03.013.

64. Pisani, P., Airoldi, M., Allais, A., Aluffi Valletti, P., Battista, M., Benazzo, M., Briatore, R., Cacciola, S., Cocuzza, S., Colombo, A., et al. (2020). Metastatic disease in head & neck oncology. Acta Otorhinolaryngol. Ital. *40*, S1–S86. https://doi.org/10.14639/0392-100X-suppl.1-40-2020.

65. Beckham, T.H., Leeman, J.E., Xie, P., Li, X., Goldman, D.A., Zhang, Z., Sherman, E., McBride, S., Riaz, N., Lee, N., and Tsai, C.J. (2019). Long-term survival in patients with metastatic head and neck squamous cell carcinoma treated with metastasis-directed therapy. Br. J. Cancer *121*, 897–903. https://doi.org/10.1038/s41416-019-0601-8.

66. Glasner, A., Ghadially, H., Gur, C., Stanietsky, N., Tsukerman, P., Enk, J., and Mandelboim, O. (2012). Recognition and prevention of tumor metastasis by the NK receptor NKp46/NCR1. J. Immunol. *188*, 2509–2515. https://doi.org/10.4049/jimmunol.1102461.

67. Merzoug, L.B., Marie, S., Satoh-Takayama, N., Lesjean, S., Albanesi, M., Luche, H., Fehling, H.J., Di Santo, J.P., and Vosshenrich, C.A.J. (2014). Conditional ablation of NKp46+ cells using a novel Ncr1greenCre mouse strain: NK cells are essential for protection against pulmonary B16 metastases. Eur. J. Immunol. *44*, 3380–3391. https://doi.org/10.1002/eji.201444643.

68. Glasner, A., Isaacson, B., Viukov, S., Neuman, T., Friedman, N., Mandelboim, M., Sexl, V., Hanna, J.H., and Mandelboim, O. (2017). Increased NK cell immunity in a transgenic mouse model of NKp46 overexpression. Sci. Rep. *7*, 13090. https://doi.org/10.1038/s41598-017-12998-w.

69. Guerra, N., Tan, Y.X., Joncker, N.T., Choy, A., Gallardo, F., Xiong, N., Knoblaugh, S., Cado, D., Greenberg, N.M., and Raulet, D.H. (2008). NKG2D-deficient mice are defective in tumor surveillance in models of spontaneous malignancy. Immunity *28*, 571–580. https://doi.org/10.1016/J.IMMUNI.2008.02.016.

70. Pasero, C., Gravis, G., Guerin, M., Granjeaud, S., Thomassin-Piana, J., Rocchi, P., Paciencia-Gros, M., Poizat, F., Bentobji, M., Azario-Cheillan, F., et al. (2016). Inherent and tumor-driven immune tolerance in the prostate microenvironment impairs natural killer cell antitumor activity. Cancer Res. *76*, 2153–2165. https://doi.org/10.1158/0008-5472.CAN-15-1965.

71. Pearce, E.L., and Pearce, E.J. (2013). Metabolic pathways in immune cell activation and quiescence. Immunity *38*, 633–643. https://doi.org/10.1016/j.immuni.2013.04.005.

72. Wang, Z., Guan, D., Wang, S., Chai, L.Y.A., Xu, S., and Lam, K.P. (2020). Glycolysis and oxidative phosphorylation play critical roles in natural killer cell receptor-mediated natural killer cell functions. Front. Immunol. *11*, 202. https://doi.org/10.3389/fimmu.2020.00202.

73. Gardiner CM. NK Cell Metabolism. doi:10.1002/JLB.MR0718-260R

74. Sheppard, S., Santosa, E.K., Lau, C.M., Violante, S., Giovanelli, P., Kim, H., Cross, J.R., Li, M.O., and Sun, J.C. (2021). Lactate dehydrogenase A-dependent aerobic glycolysis promotes natural killer cell anti-viral and anti-tumor function. Cell Rep. *35*, 109210. https://doi.org/10.1016/j.celrep.2021.109210.

75. Sun, Y., Xu, Z., Jiang, J., Xu, T., Xu, J., and Liu, P. (2020). High expression of succinate dehydrogenase subunit a which is regulated by histone acetylation, acts as a good prognostic factor of multiple myeloma patients. Front. Oncol. *10*, 563666. https://doi.org/10.3389/fonc.2020.563666.

76. Okuda, S., Watanabe, Y., Moriya, Y., Kawano, S., Yamamoto, T., Matsumoto, M., Takami, T., Kobayashi, D., Araki, N., Yoshizawa, A.C., et al. (2017). jPOSTrepo: an international standard data repository for

proteomes. Nucleic Acids Res. *45*, D1107–D1111. https://doi.org/10.1093/nar/gkw1080.

77. Darragh, L.B., Gadwa, J., Pham, T.T., Van Court, B., Neupert, B., Olimpo, N.A., Nguyen, K., Nguyen, D., Knitz, M.W., Hoen, M., et al. (2022). Elective nodal irradiation mitigates local and systemic immunity generated by combination radiation and immunotherapy in head and neck tumors. Nat. Commun. *13*, 7015. https://doi.org/10.1038/s41467-022-34676-w.

78. Sun, D., Wang, J., Han, Y., Dong, X., Ge, J., Zheng, R., Shi, X., Wang, B., Li, Z., Ren, P., et al. (2021). TISCH: A comprehensive web resource enabling interactive single-cell transcriptome visualization of tumor microenvironment. Nucleic Acids Res. *49*, D1420–D1430. https://doi.org/10.1093/nar/gkaa1020.

STAR★METHODS

KEY RESOURCES TABLE

REAGENT or RESOURCE	SOURCE	IDENTIFIER
Antibodies		
PD1-IL2v (muPD1-IL2v)	Roche	N/A
anti-CD25 (clone 7D4; TSKC22)	Roche	N/A
DP47-IL2v (DP47-muIL2v)	Roche	N/A
InVivoMAb anti-mouse CD8a (clone 53–6.7)	BioXCell	Cat#: BE0004-1, RRID: AB_1107671
InVivoMAb anti-mouse CD4 (clone GK1.5)	BioXCell	Cat#: BE0003-1, RRID: AB_1107636
InVivoMAb anti-mouse NK1.1 (clone PK136)	BioXCell	Cat#: BE0036, RRID: AB_1107737
InVivoMAb anti-mouse PD-1 (clone	BioXCell	Cat#: BE0273, RRID: AB_2687796
Purified anti-mouse CD16/CD32 FC Shield (clone 2.4G2)	Tonbo Biosciences	Cat#: 70-0161-M001, RRID: N/A
CD11b Alexa Fluor 647 (clone M1/70)	Biolegend	Cat#: 101220, RRID: AB_493546
CD11b BV650 (clone M1/70)	Biolegend	Cat#: 101239, RRID: AB_11125575
CD11b BUV661 (clone M1/70)	BD Bioscience	Cat#: 612977, RRID AB_2870249
CD11c PE-Cy5 (clone N418)	Biolegend	Cat#:117316: RRID: AB_493566
CD19 Alexa Fluor 700 (clone 6D5)	Biolegend	Cat#:115527, RRID: AB_493734
CD103 BUV395 (clone 2E7)	BD Bioscience	Cat#: 748253, RRID: AB_2872683
CD107a PerCP-eFluor710 (clone 1D4B)	eBioscience	Cat#: 46-1071-82, RRID: AB_10718968
CD122 eFluor 450 (clone TM-b1)	eBioscience	Cat#: 48-1222-82, RRID: AB_2016697
CD163 PE (clone S15049F)	Biolegend	Cat#: 156703, RRID: AB_2860724
CD25 APC/Fire 810 (clone PC61)	Biolegend	Cat#: 102075, RRID: AB_2922454
CD25 BV786 (clone C37)	BD Bioscience	Cat#: 564368, RRID: AB_2738771
CD25 PE/Dazzle 594 (clone C37)	Biolegend	Cat#: 101919, RRID: AB_2721701
CD27 BV480 (clone LG.3A10)	BD Bioscience	Cat#: 746742, RRID: AB_2744005
CD3 BUV805 (clone 17A2)	BD Bioscience	Cat#: 741982, RRID: AB_2871285
CD4 BUV496 (clone GK1.5)	BD Bioscience	Cat#: 612952, RRID AB_2813886
CD44 BV570 (clone IM7)	Biolegend	Cat#: 103037, RRID: AB_10900641
CD45 PerCP (clone 30-F11)	Biolegend	Cat#: 103130, RRID: AB_312967
CD69 Superbright 436 (clone H1.2F3)	eBioscience	Cat#: 62-0691-82, RRID: AB_2688109
CD8 BB515 (clone 53–6.7)	BD Bioscience	Cat#: 564422, RRID: AB_2738801
CD80 PerCP-Cy5.5 (clone 16-10A1)	Biolegend	Cat#: 104721, RRID: AB_893406
CXCR3 Superbright 436 (clone CXCR3-173)	eBioscience	Cat#: 62-1831-82, RRID: AB_2762747
CXCR4 eFluor 450 (clone 2B11)	eBioscience	Cat#: 48-9991-82, RRID: AB_2574143
DNAM-1 BV605 (clone TX42.1)	Biolegend	Cat#: 133613, RRID: AB_2715976
EpCAM APC (clone G8.8)	Biolegend	Cat#: 118213, RRID: AB_1134105
EpCAM BV650 (clone G8.8)	Biolegend	Cat#: 118241, RRID: AB_2876432
F4/80 BV480 (clone T45-2342)	BD Bioscience	Cat#: 565635 RRID: AB_2739313
Foxp3 Alexa Fluor 532 (clone FjK-16s)	eBioscience	Cat#: 58-5773-82, RRID: AB_11218870
Granzyme B FITC (clone QA16A02)	Biolegend	Cat#: 372205, RRID: AB_2687029
Granzyme B PE/Dazzle 594 (clone QA16A02)	Biolegend	Cat#: 372215, RRID: AB_2728382
IFNγ BUV737 (clone XMG1.2)	BD Bioscience	Cat#: 612769, RRID: AB_2870098
IL-2 APC (clone JES6-5H4)	eBioscience	Cat#: 17-7021-82, RRID: AB_469490
IL-2 BV786 (clone JES6-5H4)	Biolegend	Cat#:503843, RRID: AB_2832801
IL-10 BV711 (clone: JES5-16E3)	BD Bioscience	Cat#: 564081, RRID: AB_2738581
iNOS eFluor 450 (clone CXNFT)	eBioscience	Cat#: 48-5920-82, RRID: AB_2802293
Ki-67 APC-eF780 (clone SolA15)	eBioscience	Cat#: 47-5698-82, RRID: AB_2688065

(*Continued on next page*)

Continued

REAGENT or RESOURCE	SOURCE	IDENTIFIER
KLRG1 PerCP-Cy5.5 (clone 2F1)	BD Bioscience	Cat#: 563595, RRID: AB_2738301
LFA-1 PE (clone H155-78)	Biolegend	Cat#: 141005, RRID: AB_10694860
LFA-1 PerCP-Cy5.5 (clone H155-78)	Biolegend	Cat#: 141007, RRID: AB_10694861
Ly49A BV786 (clone A1)	BD Bioscience	Cat#: 742369, RRID: AB_ 2740727
Ly49G2 FITC (clone 4D11)	eBioscience	Cat#: 11-5781-82, RRID: AB_763604
Ly49H BUV661 (clone 3D10)	BD Bioscience	Cat#: 750512, RRID: AB_2874666
Ly6C Alexa Fluor 647 (clone HK1.4)	Biolegend	Cat#: 128009, RRID: AB_1236551
Ly6G BV421 (clone 1A8)	Biolegend	Cat#: 127627, RRID: AB_10897944
MHC II Alexa Fluor 700 (clone M5/114.15.2)	Biolegend	Cat#: 107621, RRID: AB_493726
MHC II PE/Dazzle 594 (clone M5/114.15.2)	Biolegend	Cat#:107647, RRID: AB_2565978
NK1.1 Alexa Fluor 700 (clone S17016D)	Biolegend	Cat#: 156511, RRID: AB_2892322
NKG2A PerCP-eFluor710 (clone 20d5)	eBioscience	Cat#: 46-5896-82, RRID: AB_10853352
NKG2D BV711 (clone CX5)	BD Bioscience	Cat#: 563694, RRID: AB_2722498
NKG2D Superbright 436 (clone CX5)	eBioscience	Cat#: 62-5882-82, RRID: AB_2688151
NKG2I BV421 (clone 854929)	BD Bioscience	Cat#: 748118, RRID: AB_2872579
NKp46 PE-Cy7 (clone 29A1.4)	Biolegend	Cat#: 137617, RRID: AB_11218594
NKp46 PE/Dazzle 594 (clone 29A1.4)	Biolegend	Cat#: 137629, RRID: AB_2616665
Pan-Cytokeratin Alexa Fluor 488 (clone AE-1/AE-3)	eBioscience	Cat#: 53-9003-82, RRID: AB_1834350
Pan-Cytokeratin PE (clone AE-1/AE-3)	Novus Biologicals	Cat#: NBP2-33200PE, RRID: N/A
pCD3 zeta Alexa Fluor 488 (clone 3ZBR4S)	eBioscience	Cat#: 53247841, RRID: AB_2848428
PD-1 BUV395 (clone J43)	BD Bioscience	Cat#: 744549, RRID: AB_2742320
PD-1 BUV615 (clone RMP1-30)	BD Bioscience	Cat#: 752354, RRID: AB_2875871
PD-L1 BV650 (clone MIH5)	BD Bioscience	Cat#: 740614: RRID: AB_2740313
pSTAT5 APC (clone SRBCZX)	eBioscience	Cat#: 17-9010-42, RRID: AB_2573272
pZAP70 Alexa Fluor 647 (clone 17A/P-ZAP70)	BD Bioscience	Cat#: 557817, RRID: AB_396884
Tbet BV421 (clone 4B10)	Biolegend	Cat#: 644815, RRID: AB_10896427
TCF-7/TCF-1 PE (clone S33-966)	BD Bioscience	Cat#: 564217, RRID: AB_2687845
TNFα BV750 (clone MP6-XT22)	Biolegend	Cat#: 506358, RRID: AB_2801090
Chemicals, peptides, and recombinant proteins		
Foxp3/Transcription factor staining kit	eBioscience	Cat#: 00-5523-00
Calcein, AM	Invitrogen	Cat#: C3099
Collangenase III	Worthington Biochemical	Cat#: LS004182
Live/Dead Aqua Fixable Viability Dye	Invitrogen	Cat#: L34966
RBC Lysis Buffer	eBioscience	Cat#: 00-4333-57
DAPI	Biolegend	Cat#: 422801
Critical commercial assays		
EasySep Mouse $CD8^+$ T cell isolation kit	StemCell Technologies	Cat#: 19853
EasySep Mouse NK Cell Isolation Kit	StemCell Technologies	Cat#: 19855
Human IL-2 ELISA Kit Picokine	Boster Bio	Cat#: EK0397
Deposited data		
CD8 Proteomics	This paper	jPOST: PXD043110
NK cell Proteomics	This paper	jPOST: PXD043109
RNA seq dataset	Darragh et al.[31] https://doi.org/10.1038/s43018-022-00450-6	GEO: GSE210287
Experimental models: Cell lines		
MOC2	Provided by R. Uppaluri	RRID: CVCL_ZD38
LY2		RRID: CVCL_Z594
P029	Provided by X.J. Wang	N/A

(*Continued on next page*)

Continued

REAGENT or RESOURCE	SOURCE	IDENTIFIER
Experimental models: Organisms/strains		
Mouse: C57BL/6J	Jackson Laboratories	Strain Code: 000664
Mouse Balb/C	Charles River	Strain Code: 028
Software and algorithms		
Flowjo (v10.8.1)	BD Bioscience	https://www.flowjo.com
Grahpad Prism (v9)	Dotmatics	https://www.graphpad.com
Amnis IDEAS (v6.2)	Luminex	https://www.Luminexcorp.com
Cytobank	Beckman Coutler	https://premium.cytobank.org/cytobank
R (version 4.0)	The R Foundation	https://www.r-project.org

RESOURCE AVAILABILITY

Lead contact

Further information and requests for resources and reagents should be directed to the lead contact, Sana D. Karam (sana.karam@cuanschutz.edu).

Materials availability

This study did not generate any new, unique reagents.

Data and code availability

- CD8 and NK cell proteomics dataset generated for this manuscript has been deposited in the ProteomeXchange Consortium via jPOST Repository[76] (jPOST: PXD043109, jPOST: PXD043110)
- This paper does not report any original code.
- Any additional information required to reanalyze the data reported in this work paper is available from the lead contact upon request.

EXPERIMENTAL MODEL AND SUBJECT PARTICIPANT DETAILS

Cell lines

MOC2 (female), LY2 (male), and P029 (female) murine squamous cell carcinoma cells lines were used for the *in vivo* studies. Cell lines were cultured in appropriate media; DMEM-F12 with 10% FBS and 1% primocin/fungin for LY2 and P029, and a 1:2 mixture of DMEM-F12/IMDM supplemented with 10% FBS and 1% primocin/fungin, 1.75 μg EGF, 20ug hydrocortisone, and 0.1% insulin for MOC2, as previously reported. P029 cell line was provided in collaboration with XJ Wang at University of Colorado Anschutz Medical Campus, Department of Pathology.[77]

Mouse models

C57Bl/6 and Balb/c mice were obtained from the Jackson Laboratory (Bar Harbor, Maine, USA) and Charles River (Wilmington, MA, USA) respectively and were used for MOC2, P029, and LY2 *in vivo* studies. For experimentation, mice were 6–8 weeks old, and age/gender matched when appropriate. Mice were housed under pathogen free conditions with a maximum of 5 per cage, with all protocols for animal models were approved by the Institutional Animal Care and Use Committee (IACUC) of the University of Colorado Anschutz Medical Campus.

Tumor studies

Murine MOC2, LY2, and P029 were implanted orthotopically into the buccal mucosa as previously described.[7] Mice were appropriately age matched and were randomized into groups, with treatment beginning when tumor volume was approximately 150 mm^3. Tumor measurements were conducted twice weekly using digital calipers, with tumor volume was calculated as $V= (AxB^2)/2$. A is measured as the short diameter and B as the long diameter. For tumor studies the following cell numbers were implanted into the buccal mucosa: MOC2 cell line 1×10^5 cells were implanted per mouse, LY2 1×10^6 cells were implanted per mouse, and for P029 5×10^4 cells were implanted per mouse. Primary tumor, serum, and lungs were harvested at the time of sacrifice. *In vivo* experiments were independently repeated and verified to validate results.

Human patient samples

Human samples were obtained from HNSCC patients from a completed phase I/Ib clinical trial (NTC:03635164) at the University of Colorado Denver. Samples were obtained from 21 patients, from 43 to 84 years of age, with an average age of 61 years. Of the enrolled patients seven were female, and 14 were male, with a life expectancy $\geq$24 weeks, and diagnosed with intermediate and high-risk p16-negative, stages III and IV, nonmetastatic HNSCC cancer that was deemed resectable or borderline resectable by an Otolaryngology surgeon. Diagnosis was confirmed as stage III or IV head and neck squamous cell carcinoma of oral cavity, hypopharynx, oropharynx, or larynx before enrollment in the trial as reported in Darragh et al.[31] Tumor tissue collected from the initial biopsy and time of surgery was used for RNA sequencing. Blood taken from patients was processed to collect PBMC's and plasma. Written, inform consent was obtained from all participants prior to performing any procedures.

METHOD DETAILS

Antibodies and drugs

αCD25, PD1-IL2v, and DP47-IL2v were provided in collaboration with Roche Pharmaceuticals. αCD25 was given at a concentration of 3 mg/kg, PD1-IL2v and DP47-IL2v were given at a concentration of 0.5 mg/kg. Antibodies were administered weekly via I.P. injection beginning one day prior to the beginning of RT. For studies not utilizing radiation therapy, I.P. injections were administered after tumor implantation, at a time point equivalent to one day before RT. aPD-1, αCD4, αCD8, and αNK1.1 were administered twice weekly at 10 mg/kg via I.P. injections. CD8. CD4, and NK cell depletion was verified using flow cytometric analysis. All dilutions were made using sterile DPBS.

Irradiation

Irradiation was performed using the PXi-225Cx image guided irradiator at 225kV, 20mA with a 0.3 mm Cu filter. Mice were anesthetized with vaporized isoflurane and placed in the prone position, and RT was delivered at a dose rate of 5.6 Gy/min. Dose rates are checked monthly using an ionization chamber and CBCT scans were acquired to determine accurate positioning of mice. The irradiation plan was based on Monte Carlo simulations of a mouse model.

Flow cytometry

Tumor, blood, and tumor draining lymph nodes were harvested and processed for flow cytometric analysis. Tumor tissue was chopped and incubated in Collagenase III (Worthington) for 30 min at 37°C. After incubation, tissue was passed through a 70um nylon cell strainer to produce a single cell suspension. After centrifugation, red blood cells were lysed using RBC lysis buffer (Invitrogen), using HBSS to neutralize the lysis buffer. Lymph nodes were similarly processed by mechanical separation into single cell suspension. Blood was immediately centrifuged after collection and resuspended in RBC lysis buffer as described above. Cells were transferred into 24 well plates and incubated with monensin and brefeldin to prevent release of cytokines, and stimulated with PMA/ionomycin cocktail for 4 h at 37°C. Following incubation, cells were incubated in FC block (CD16/CD32 antibody, Tonbo bioscience) for 15 min at 4°C. Cells were then incubated in Live/Dead Fixable Aqua Viability Stain Kit (Invitrogen) in the dark for 20 min at 4°C. Cells were then stained for surface markers and incubated for 20 min at 4°C. For analysis of immune cells, the following antibodies were: PerCP–CD45 (clone: 30-F11, Biolegend), BUV805–CD3 (clone: 17A2, BD Biosciences), BUV 496-CD4 (clone: GK1.5, BD Biosciences), BB515-CD8 (clone: 53–6.7, BD Biosciences), BV570-CD44 (clone: IM7, Biolegend), PE-Cy7-NKp46 (clone: 29A1.4, Biolegend), Superbright 436-CD69 (clone: H1.2F3, eBioscience), BV605-DNAM-1 (clone: TX42.1, Biolegend), BV786-CD25 (clone: 3C7, BD Biosciences), BUV395-PD-1 (clone: J43, BD Biosciences), BV650-PD-L1 (clone: MIH5, BD BioSciences), PE-Cy5-CD11c (clone: N418, Biolegend), PE/Dazzle 594-MHC II (clone M5/114.15.2, Biolegend), PerCP-Cy5.5-CD80 (clone: 16-10A1, Biolegend), BUV661-CD11b (clone: M1/70, BD Biosciences), Alexa Fluor 647-Ly6C (clone: HK1.4, Biolegend), BV421-Ly6G (clone: 1A8, Biolegend), Alexa Fluor 700-CD19 (clone: 6D5, Biolegend), BV480-F4/80 (clone: T45-2342), eFluor 450-iNOS (clone: CXNFT, eBioscience), PE-CD163 (clone: S15049F, Biolegend), APC-eFluor 780-Ki-67 (clone: SolA15, eBioscience), Alexa Fluor 532-Foxp3 (clone: FjK-16s, eBioscience), APC-IL-2 (clone: JES6-5H4, eBioscience), BUV737-IFNγ (clone: XMG1.2, BD Biosciences), FITC-Granzyme B (clone: QA16A02, Biolegend), BV750-TNFα (clone: MP6-XT22, Biolegend), BV711-IL-10 (clone: JES5-16E3, BD Bioscience), PE-pan-cytokeratin (clone: AE-1/AE-3, Novus Biologicals), BV650-EpCAM (clone: G8.8, Biolegend), Alexafluor 488-pan cytokeratin (clone: AE1/AE3, Invitrogen) Alexafluor 700-NK1.1 (clone: S17016D, Biolegend), eFluor450-CD122 (clone: TM-b1, eBioscience), PE/Dazzle594-CD25 (clone: C37, Biolegend), Alexafluor 647-CD11b (clone: M1/70, Biolegend), BV711-NKG2D (clone: CX5, BD Bioscience), PerCP-eFluor 710-NKG2A (clone: 20d5, eBioscience), BUV661-Ly49H (clone: 3D10, BD Bioscience), PerCP-Cy5.5-KLRG1 (clone: 2F1, BD Bioscience), PE-LFA-1 (clone: H155-78, Biolegend), Superbright 436-CXCR3 (clone: CXCR3-173, eBioscience), BV421-NKG2I (clone: 854929, BD Bioscience), FITC-Ly49G2 (clone: 4D11, eBioscience), BV786-Ly49A (clone: A1, BD Bioscience), AP/Fire 810 -CD25 (clone PC61, Biolegend), BV480-CD27 (clone LG.3A10, BD Bioscience), BV650-CD11b (clone M1/70, Biolegend), Superbright 436-NKG2D (clone CX5, eBioscience), BUV615-PD-1 (clone RMP1-30, BD Bioscience), PerCP-eFluor710-CD107a (clone 1D4B, eBioscience), PerCP-Cy5.5-LFA-1 (clone H155-78, Biolegend), Alexa Fluor 700-MHC II (clone M5/114.15.2, Biolegend), BUV395-CD103 (clone 2E7, BD Bioscience), eFluor 450-CXCR4 (clone 2B11, eBioscience), Alexa Fluor 647, pZAP70 (clone 17A/P-ZAP70, BD Bioscience), APC-pSTAT5 (clone SRBCZX, eBioscience), BV785-IL-2 (clone JES6-5H4, Biolegend), PE-TCF-7/TCF-1 (clone S33-966, BD Bioscience), PE/Dazzle 594-Granzyme B (clone QA16A02, Biolegend), BV421-Tbet (clone 4B10,

Biolegend), Alexa Fluor 488-pCD3 zeta (clone 3ZBR4S, eBioscience). After surface staining, cells were fixed and permeabilized using the Foxp3 perm/fix kit (Invitrogen) overnight. Following incubation, cells were stained for intracellular markers and incubated for 30 min at 4°C. Samples were then run on a Cytek Aurora spectral cytometer at the University of Colorado Diabetes Research Center Flow Cytometry Core. Fluorescence minus one control were used to determine gating strategy. Flowjo analysis software was used for data analysis.

Immunohistochemistry and H&E staining

Lungs were harvested at time of sacrifice and fixed in 10% buffered Formalin. Tissue was submitted to University of Colorado Anschutz Medical Campus, Gates Center for Regenerative Medicine Histology Core where slides were cut, mounted, and H&E stained. Tissue was mounted using every 3rd cut.

Human pathways analysis and mass cytometry analysis

Data was gathered from a recently completed phase I/Ib clinical trial (NTC:03635164). Patients were treated with neoadjuvant durvalumab and stereotactic body radiation therapy (SBRT). Tumor tissue and blood was collected pre and post treatment and processed for bulk RNA sequencing and immunophenotyping via mass cytometry (CyTOF).

Gene set enrichment analysis on bulk RNA sequencing was performed using the full ranked list of genes by $\log_2$ fold change on Kyoto Encyclopedia of Genes and Genomes (KEGG) pathways.

NK cytotoxicity assay

NK cells were harvested and isolated from the blood of tumor bearing C57BL/6 mice using an NK negative selection isolation kit (Stemcell). P029 tumor cells were stained with calcein (Thermofisher) at a concentration of 2 μg/mL in RPMI media with 10% FBS. NK cells and P029 tumor cells were incubated together at a 2:1 ratio of NK to tumor cells and incubated at 37°C for 4 h. After incubation plates were centrifuged and supernatant was removed and transferred to 96 well plate. Plates were read on Tecan Infinite M plex fluorescence plate reader at 485 nm excitation and 530 nm emission. Cell lysis was calculated using the following equation : $[(\textit{Test release} - \textit{spontaneous release})/(\textit{Maximum release} - \textit{spontaneous release})]\,x\,100$. Maximum release was calculated by incubating P029 tumor cells with solution of 1% Triton X-100 in RPMI and spontaneous release was calculated by incubating cells in incubation media without stimulus added.

Imagestream cytometry

NK cells were harvested and isolated from spleens of tumor bearing mice. Processed into single cell suspension following above protocol, and NK were isolated using an NK isolation kit (Stemcell) following manufacturer's instructions. Isolated NKs were then stained using the following antibodies: APC-EpCAM, PE/Dazzle 594- NKp46 (Biolegend), FITC-Granzyme B (Biolegend). Nuclei were stained using 4′6-diamidino-2-phenylindole (DAPI). Following staining, cells were washed and resuspended in PBS and processed through Amnis Imagestream X Mk II imaging flow cytometer (Amnis, Seattle, WA). Analysis was performed using IDEAS 6.2 software (AMNIS, Seattle, WA).

Proteomics

Blood from tumor bearing mice was collected and processed into a single cell suspension as described above. After processing, CD8 and NK cells were isolated using a CD8 T cell (Stemcell) and NK cell negative isolation kits following manufacturer's instructions. Isolated cells were then stained with PE-CD8 and APC-NKp46 and then cell sorted to achieve a pure single cell population. Cell sorting was performed using a Beckman Coulter MoFlo XDP750 (Beckman Coutler). High-throughput proteomic analysis was performed at the University of Colorado School of Medicine Proteomics Facility on murine serum samples. The samples were digested according to the FASP protocol using a 10 kDa molecular weight cutoff filter. In brief, the samples were mixed in the filter unit with 8 M urea, 0.1M ammonium bicarbonate (AB) pH 8.0, and centrifuged at 14 000 g for 15 min. The proteins were reduced with 10 mM DTT for 30 min at RT, centrifuged, and alkylated with 55 mM iodoacetamide for 30 min at RT in the dark. Following centrifugation, samples were washed 3× with urea solution, and 3× with 50 mM AB, pH 8.0. Protein digestion was carried out with sequencing grade modified Trypsin (Promega) at 1/50 protease/protein (w/w) at 37°C overnight. Peptides were recovered from the filter using 50mM AB. A 20 μl of each sample was loaded onto individual Evotips for desalting and then washed with 20 μL 0.1% FA followed by the addition of 100 μL storage solvent (0.1% FA) to keep the Evotips wet until analysis. The Evosep One system ((Evosep, Odense, Denmark) was used to separate peptides on a Pepsep column, (150 μm inter diameter, 15 cm) packed with ReproSil C18 1.9 μm, 120A resin. The system was coupled to the timsTOF Pro mass spectrometer (Bruker Daltonics, Bremen, Germany) via the nano-electrospray ion source (Captive Spray, Bruker Daltonics). The mass spectrometer was operated in PASEF mode. The ramp time was set to 100 m and 10 PASEF MS/MS scans per topN acquisition cycle were acquired. MS and MS/MS spectra were recorded from m/z 100 to 1700. The ion mobility was scanned from 0.7 to 1.50 Vs./cm^2. Low-abundance precursor ions with an intensity above a threshold of 500 counts but below a target value of 20000 counts were repeatedly scheduled and otherwise dynamically excluded for 0.4 min. The identification settings were as follows: Trypsin, Specific, with a maximum of 2 missed cleavages, up to 2 isotope errors in precursor selection allowed for, 10.0 ppm as MS1 and 0.4 Da as MS2 tolerances; fixed modifications: Carbamidomethylation of

C (+57.021464 Da), variable modifications: Oxidation of M (+15.994915 Da), Acetylation of protein N-term (+42.010565 Da), Pyrolidone from peptide N-term Q or C (−17.026549 Da). Graphs were rendered using GraphPad Prism (9.3.1).

Human single cell RNA sequencing analysis

Comparative gene expression and annotated cell maps from human single cell RNA sequencing datasets were generated using the Tumor Immune single cell hub (TISCH) database.[78] Puram et al. (GEO: GSE103322)[25] and Cillo et al. (GEO: GSE139324)[26] were head and neck single cell datasets included in analysis.

Dimensionality reduction algorithms and self organized mapping

Plots using viSNE or FlowSOM analysis was performed using the Cytobank analysis software (Beckman Coulter). CD45 positive cells were identified using PerCP stain. Positive cells were downsampled to remove sample bias and concatenated into a single file. Concatenated files for each treatment group were run through Cytobank viSNE dimensionality reduction analysis tool. After generating viSNE, files were then separated into clusters using flowSOM clustering algorithm. Populations were assigned and identified using depending on histogram and heatmap expression.

Cytokine quantification

IL-2 plasma concentrations of human clinical trial patients were determined using an ELISA assay (Boster Bio). Assay was performed using manufacturer's instructions.

QUANTIFICATION AND STATISTICAL ANALYSIS

All statistical analyses were processed using GraphPad Prism v9. Statistical analysis was completed using one-way analysis of variance (one-way ANOVA) with Tukey correction for comparisons with 3 or more groups, and unpaired t-tests for comparisons using only two groups. Kaplan-Meier curves were used for survival analysis, using log-ranked (Mantel-Cox) test for comparisons of all groups. Data is represented as mean SEM, unless otherwise noted. Statistical significance is indicated as *$p < 0.05$, **$p < 0.005$, ***$p < 0.0005$, ****$p < 0.0001$.

ADDITIONAL RESOURCES

RNA sequencing in this manuscript is associated with a phase I/Ib clinical trial (NTC03635164).